NAVAL POSTGRADUATE SCHOOL
MONTEREY, CALIFORNIA

THESIS

TRANSIENT LOCALIZATION IN SHALLOW WATER ENVIRONMENTS

by

Joachim Brune

March 1998

Thesis Co-Advisors: Kevin B. Smith
Ching-Sang Chiu
Ralph Hippenstiel

Approved for public release; distribution is unlimited.

REPORT DOCUMENTATION PAGE

Form Approved OMB No. 0704-0188

1. AGENCY USE ONLY *(Leave blank)*	2. REPORT DATE March 1998	3. REPORT TYPE AND DATES COVERED Master's Thesis

4. TITLE AND SUBTITLE TRANSIENT LOCALIZATION IN SHALLOW WATER ENVIRONMENTS

5. FUNDING NUMBERS

6. AUTHOR(S) Joachim Brune

7. PERFORMING ORGANIZATION NAME(S) AND ADDRESS(ES)
Naval Postgraduate School
Monterey, CA 93943-5000

8. PERFORMING ORGANIZATION REPORT NUMBER

9. SPONSORING/MONITORING AGENCY NAME(S) AND ADDRESS(ES)

10. SPONSORING/MONITORING AGENCY REPORT NUMBER

11. SUPPLEMENTARY NOTES The views expressed in this thesis are those of the author and do not reflect the official policy or position of the Department of Defense or the U.S. Government.

12a. DISTRIBUTION/AVAILABILITY STATEMENT
Approved for public release; distribution is unlimited.

12b. DISTRIBUTION CODE

13. ABSTRACT *(maximum 200 words)*

In this work, the robustness of a simple, Bartlett-type processor based on matching broadband signal autocorrelation functions is investigated. Measures of robustness to be examined include the size of the localization footprint on the ambiguity surface and the peak-to-sidelobe levels in the presence of environmental mismatch and noise. A full-wave PE model is used to produce broadband replicas. Both model-generated synthetic signals, which provide baseline results, and measured pulses in a shallow water environment are analyzed.

This work suggests that environmental mismatch has a more significant effect on the localization performance than noise. It also suggests that, as long as the noise level is not higher than the signal level, the localization performance will not be significantly affected. This is to be expected, since for white noise the majority of the influence on the autocorrelation function occurs at zero lag which has been removed in the localization algorithms. It is also shown that the autocorrelation matching in the time-domain is generally more useful for smaller bandwidths at low frequencies, which has been observed in previous work, whereas the autocorrelation matching in the frequency-domain is better suited for larger bandwidths and higher frequencies.

14. SUBJECT TERMS Autocorrelation Matching, Transient Localization, Shallow Water

15. NUMBER OF PAGES 85

16. PRICE CODE

17. SECURITY CLASSIFICATION OF REPORT	18. SECURITY CLASSIFICATION OF THIS PAGE	19. SECURITY CLASSIFICATION OF ABSTRACT	20. LIMITATION OF ABSTRACT
Unclassified	Unclassified	Unclassified	UL

Approved for public release; distribution is unlimited.

TRANSIENT LOCALIZATION IN SHALLOW WATER ENVIRONMENTS

Joachim Brune
Lieutenant, German Navy
B.S., University of German Armed Forces Hamburg, 1990

Submitted in partial fulfillment
of the requirements for the degrees of

MASTER OF SCIENCE
IN
ELECTRICAL ENGINEERING AND ENGINEERING ACOUSTICS

from the

NAVAL POSTGRADUATE SCHOOL
March 1998

Author: _____
Joachim Brune

Approved by: _____
Kevin B. Smith, Thesis Co-Advisor, Chairman Engineering Acoustics Academic Committee

_____
Ching-Sang Chiu, Co-Advisor

_____
Ralph Hippenstiel, Co-Advisor

_____
Herschel H. Loomis, Jr., Chairman
Department of Electrical and Computer Engineering

ABSTRACT

In this work, the robustness of a simple, Bartlett-type processor based on matching broadband signal autocorrelation functions is investigated. Measures of robustness to be examined include the size of the localization footprint on the ambiguity surface and the peak-to-sidelobe levels in the presence of environmental mismatch and noise. A full-wave PE model is used to produce broadband replicas. Both model-generated synthetic signals, which provide baseline results, and measured pulses in a shallow water environment are analyzed.

This work suggests that environmental mismatch has a more significant effect on the localization performance than noise. It also suggests that, as long as the noise level is not higher than the signal level, the localization performance will not be significantly affected. This is to be expected, since for white noise the majority of the influence on the autocorrelation function occurs at zero lag which has been removed in the localization algorithms. It is also shown that the autocorrelation matching in the time-domain is generally more useful for smaller bandwidths at low frequencies, which has been observed in previous work, whereas the autocorrelation matching in the frequency-domain is better suited for larger bandwidths and higher frequencies.

TABLE OF CONTENTS

I. INTRODUCTION

Acoustic source localization has been an intensive research issue for the past few decades. Prior to that, passive SONAR was used to obtain an estimate of the source direction and other techniques, such as Target Motion Analysis (TMA), and Contact Motion Analysis (CMA), were used to get an estimate of the range to the source. With the introduction of faster computers other possibilities arose.

One of the techniques that was developed is known as Matched Field Processing (MFP). The MFP process consists of systematically placing a synthetic source at each point in a search grid and comparing the signal parameters estimated for all the synthetic source locations with the signal parameters of the true source (Tolstoy, 1993). When the synthetic source location and the true source location match, the correlation of the true and the synthetic received signal should be a maximum. Most of the work in this field has been done with array receivers and narrow band signals. This work deals with a single receiver hydrophone and broadband signals. Pioneering work in this field has mainly been done by Clay in the 1960's and 70's (Clay, 1987).

The objective of this study is an examination of the influence of the propagation mismatch due to environmental uncertainty on a number of MFP algorithms for a single hydrophone receiver and a transient-like point source. Several aspects of environmental mismatch can be independently evaluated providing information of localization performance as a function of model degradation. Time-domain signal autocorrelation matching and frequency-domain autocorrelation matching are performed to produce the ambiguity surface for the localization.

Measures of robustness of the algorithms to be examined include the size of the footprint on the ambiguity surface and the peak-to-sidelobe levels in the presence of environmental mismatch. A full-wave, parabolic equation model is employed to produce broadband replica signals. Both model-generated synthetic signals, which provide baseline results, and measured pulses in a shallow water environment are analyzed. A secondary but

no less important objective is to suggest directions for future research beyond the present available algorithms.

The remainder of this thesis consists of five chapters. Chapter II describes the acoustic propagation model and arrival structure synthesis. Chapter III describes the matching algorithms and the interface of the arrival structure synthesis with these algorithms. Chapter IV describes the setup of the experiments and the numerical results of the matching algorithms. Chapter V describes the analysis of real broadband data with the matching algorithms. Chapter VI presents the conclusions of the study and describes issues which were encountered during the research and were not investigated, but which may lead to more robust algorithms.

II. THE PE-PROPAGATION MODEL AND ARRIVAL STRUCTURE SYNTHESIS

A. THE PARABOLIC EQUATION MODEL

In order to predict the arrival structure at a receiver location due to a point source at a test location, an acoustic propagation model must be employed. Throughout this work, the Monterey-Miami Parabolic Equation (MMPE) model (Smith, 1996) has been used to produce the synthetic signals. In this chapter, the general theory of the parabolic equation model is presented. The methods for processing the outputs of the model to produce the time-domain arrival structure predictions are also described.

We begin with the inhomogeneous wave equation for the acoustic pressure $p(\vec{x},t)$ in a medium with sound speed $c(\vec{x})$ and density $\rho(\vec{x})$ (Jensen et al., 1994)

$$\rho(\vec{x})\nabla\cdot\left(\frac{\nabla p(\vec{x},t)}{\rho(\vec{x})}\right)-\frac{1}{c(\vec{x})^2}\frac{\partial^2 p(\vec{x},t)}{\partial t^2}=S(\vec{x}_s,t). \tag{1}$$

The parabolic equation model is based on an approximation to the Helmholtz wave equation in a cylindrical coordinate system. The majority of the ocean environment is well suited for a description in cylindrical coordinates. Assuming a time harmonic solution, the Helmholtz equation in cylindrical coordinates takes the form (see, e.g., Jensen et al., 1994)

$$\begin{aligned}&\frac{1}{r}\frac{\partial}{\partial r}\left(r\frac{\partial p_f(r,z,\phi)}{\partial r}\right)+\frac{1}{r^2}\frac{\partial^2 p_f(r,z,\phi)}{\partial \phi^2}+\frac{\partial^2 p_f(r,z,\phi)}{\partial z^2}\\&+k_0^2 n^2(r,z,\phi)p_f(r,z,\phi)\\&=-4\pi P_0\delta(\vec{r}-\vec{r}_S)\end{aligned}, \tag{2}$$

where

$p(r,z,\phi,f,t)=p_f(r,z,\phi)e^{-i2\pi ft}$, $k_0=\frac{\omega}{c_0}$ is a reference wavenumber and the acoustic index of refraction is defined by

$$n=\frac{c_0}{c(r,z,\phi)}. \tag{3}$$

Note that we have assumed the density is constant in this derivation. The influence of density contrasts at the water-bottom interface can easily be included by defining an effective index of refraction which contains the appropriate additional terms (see, e.g., Tappert, 1977).

As energy is primarily radiating outward from the source, $p_f(r,z,\phi)$ can be approximated by

$$p_f(r,z,\phi) = \psi_f(r,z,\phi)H_0^{(1)}(k_0 r), \tag{4}$$

where $\psi_f(r,z,\phi)$ is a slowly varying envelope and $H_0^{(1)}(k_0 r)$ is the Hankel function of the first kind. In the far-field, we can take advantage of the asymptotic approximation of the Hankel function and re-write Eq.(4) as

$$p_f(r,z,\phi) = \frac{P_0 R_0}{\sqrt{r}}\psi(r,z,\phi)e^{ik_0 r}, \tag{5}$$

normalized such that at $r = R_0$, $|p_f| = P_0$. Substituting this into Eq. (2) yields

$$\frac{\partial^2 \psi}{\partial r^2} + i2k_0\frac{\partial \psi}{\partial r} + \frac{1}{r^2}\frac{\partial^2 \psi}{\partial \phi^2} + \frac{\partial^2 \psi}{\partial z^2} + \left[k_0^2(n^2-1) + \frac{1}{4r^2}\right]\psi = 0, \tag{6}$$

where the source function on the right-hand side has been dropped for simplicity. The influence of the source term is only significant at range r = 0, and can be accounted for with the proper definition of the starting field. Neglecting the azimuthal coupling and the near-field terms, and assuming that ψ is a slowly varying function with range, we arrive at

$$\frac{\partial \psi}{\partial r} = \frac{i}{2k_0}\frac{\partial^2 \psi}{\partial z^2} + \frac{ik_0}{2}(n^2-1)\psi. \tag{7}$$

Defining the operators

$$T_{op} = -\frac{1}{2k_0}\left(\frac{\partial^2}{\partial z^2}\right), \tag{8}$$

and

$$U_{op} = -\frac{1}{2}(n^2-1), \tag{9}$$

Eq.(7) can be written as

$$ik_0^{-1}\frac{\partial \psi}{\partial r} = \left(T_{op} + U_{op}\right)\psi \,. \tag{10}$$

With the operators defined above, this constitutes what is commonly referred to as the "standard" parabolic equation (SPE) (Tappert, 1977). For this work, we have employed the higher order "wide angle" parabolic equation (WAPE) (Thomson and Chapman, 1983) with operators defined by

$$T_{WAPE} = -\frac{1}{k_0^2}\frac{\partial^2}{\partial z^2}\left[\left(1+\frac{1}{k_0^2}\frac{\partial^2}{\partial z^2}\right)^{1/2}+1\right]^{-1}, \tag{11}$$

and

$$U_{WAPE} = -(n-1)\,. \tag{12}$$

A split-step Fourier algorithm is used to numerically integrate the solution in range. This involves alternatively applying the U_{op} and the T_{op} operators in the z-domain and the k_z-domain, respectively, where each operator is simply a scalar multiplier. The algorithm for stepping in range from r to $r+\Delta r$ can then be succinctly expressed as

$$\psi(r+\Delta r, z) = e^{-ik_0 \Delta r U_{op}(r,z)} \cdot FFT\left(e^{-ik_0 \Delta r \hat{T}_{WAPE}(r,k_z)} \cdot \left[FFT\left(\psi^*(r,z)\right)\right]^*\right), \tag{13}$$

where the wide angle $\hat{T}_{WAPE}$ operator in the k_z-space is defined as

$$\hat{T}_{WAPE}(k_z) = 1 - \sqrt{\left(1-\frac{k_z^2}{k_0^2}\right)}\,. \tag{14}$$

Note that the FFT convention used here is consistent with the form defined by [Press, et al.,1988]. The calculation of the inverse FFT is accomplished by a forward FFT and a double conjugation.

The output of the model is in the form of the field functions ψ (magnitude and phase) and has been referenced to a unity magnitude at 1 m. The field is only computed at discrete points and the spacing in depth and range are the primary parameters that determine the accuracy of the results. The wavelength of interest in this study is between 0.7 and 3 m and the grid spacing used is 40 cm in depth and 50 cm in range. Note that the grid size is

about $\lambda/2$ which is necessary to obtain the highest accuracy up to ± 90 degrees propagation angles. This oversampling of the acoustic field was chosen to provide maximum information in the generation of the ambiguity surfaces.

B. PE-ARRIVAL STRUCTURES

The pressure is defined in terms of the PE field function, as stated in Eq. (6), by

$$p(r,z,f) = \frac{P_0}{\sqrt{r}} R_0 e^{ik_0 r} \psi(r,z,f), \tag{15}$$

where P_0 is the amplitude of the source pressure measured at $R_0 = 1\,\mathrm{m}$. The broadband results were obtained by running the model multiple times for all discrete frequencies in the bandwidth under consideration and then performing a Fourier synthesis to yield travel time results. In order to make this work a multiplication by some window-function is necessary. Assuming a normalized source amplitude, the complex arrival structure of the pressure field can then be written as

$$\begin{aligned} p(r,z,t) &= \int_{-\infty}^{\infty} p(r,z,f) e^{-i2\pi ft} df \\ &= \frac{1}{\sqrt{r}} \int_{-\infty}^{\infty} e^{ik_0 r} \psi(r,z,f) e^{-i2\pi ft} df \end{aligned} \tag{16}$$

Since $e^{ik_0 r} = e^{i2\pi f \frac{r}{c_0}}$, this phase factor can be neglected by defining the reduced time $T = t - \left(\frac{r}{c_0}\right)$ such that

$$p(r,z,T) = \frac{1}{\sqrt{r}} \int_{-\infty}^{\infty} \psi(r,z,\phi) e^{-i2\pi fT} df\,. \tag{17}$$

Note that using a reduced time has no influence on the autocorrelation function.

III. LOCALIZATION ALGORITHMS

The Transient Localization Project at the Naval Postgraduate School has in recent years studied different localization algorithms for the scenario of one receiver hydrophone and a point source. All the routines were based on fundamental concepts of generalized correlation functions described in Bendat and Piersol, 1971, and most of them are described in Miller et al., 1996, Hager, 1997, and Pierce, 1996.

Localization algorithms may be considered generalized beamformers in which the plane wave replicas have been replaced by more complicated replicas of the acoustic propagation (e.g., modes, beams, or the vertical pressure field). The algorithms, usually referred to as processors, are in most cases based on a Hermitian quadratic product. The exact form is determined by the constraints that are put on the processor output.

All localization algorithms are based on matching the received signal with a replica. Replicas are simulated received signals of synthetic sources at a large number of gridpoints in a search space. When the propagation model is 100% correct, and the synthetic and real source functions are equal, the real and synthetic received signal should exactly match where the real and synthetic source positions coincide. Results of the localization are usually presented as an ambiguity surface. All MFP algorithms are based on this principle in some form.

All the localization algorithms described below are applicable to the single hydrophone case but can easily be extended to an array of hydrophones. The source is assumed to be omnidirectional. Using the reciprocity principle reduces the amount of work to a manageable size, and makes localization possible in a reasonable and operationally feasible time. The reciprocity principle states that in an environment without time variations (e.g., currents) the acoustic pressure at location B from an omnidirectional source at location A and the acoustic pressure at A from an equivalent source at B are identical if the densities at A and B are the same. The replicas may, therefore, be generated from predictions of the acoustic propagation outward from the receiver location to all possible source locations in the search grid.

A. TIME-DOMAIN AUTOCORRELATION MATCHING (TACM)

Assuming a transient arrival, which can be described by the complex pressure time series $P(t)$, is detected, the autocorrelation of the complex, time-domain signal is defined as

$$T_{pp}(\tau) = \int_{-\infty}^{\infty} P^*(t)P(t+\tau)dt\,. \tag{18}$$

In terms of the frequency-domain response, this can be written as (Proakis, and Manolakis, 1996)

$$\tilde{P}(f) = \int_{-\infty}^{\infty} P(t)e^{i2\pi ft}dt, \tag{19}$$

so Eq. (18) becomes

$$T_{pp}(\tau) = \int_{-\infty}^{\infty} \tilde{P}^*(f)\tilde{P}(f)e^{-i2\pi f\tau}df\,. \tag{20}$$

Normalization of the autocorrelation produces

$$C_{pp}(\tau) = \frac{T_{pp}(\tau)}{\int_{-\infty}^{\infty}\left|\tilde{P}(f)\right|^2 df}. \tag{21}$$

Note that the autocorrelation function defined by Eq. (21) is a complex quantity.

For a given predicted replica signal, the normalized autocorrelation function is similarly defined by

$$C_{RR}(\tau) = \frac{T_{rr}(\tau)}{\int_{-\infty}^{\infty}\left|\tilde{R}(f)\right|^2 df}. \tag{22}$$

Note that this function is also complex.

The autocorrelation matching algorithm is based upon the inner product of the two functions defined by Eqs. (21) and (22). With proper normalization, this is

$$A_{RP} = \frac{\int_{-\infty}^{\infty} C_{RR}^*(\tau)C_{PP}(\tau)d\tau}{\left[\int_{-\infty}^{\infty}\left|C_{RR}(\tau)\right|^2 d\tau \int_{-\infty}^{\infty}\left|C_{PP}(\tau)\right|^2 d\tau\right]^{1/2}}. \tag{23}$$

Since

$$\int_{-\infty}^{\infty} C_{RR}^{*}(\tau) C_{PP}(\tau) d\tau = \int_{-\infty}^{\infty} d\tau \left[\int_{-\infty}^{\infty} df \left| \tilde{R}(f) \right|^2 e^{-i2\pi f\tau} \right] \left[\int_{-\infty}^{\infty} df' \left| \tilde{P}(f') \right|^2 e^{-i2\pi f\tau} \right]$$

$$= \int_{-\infty}^{\infty} df' \left| \tilde{P}(f') \right|^2 \int_{-\infty}^{\infty} df \left| \tilde{R}(f) \right|^2 \left[\int_{-\infty}^{\infty} d\tau e^{-i2\pi(f-f')\tau} \right] \quad , \quad \textbf{(24)}$$

$$= \int_{-\infty}^{\infty} df \left| \tilde{R}(f) \right|^2 \left| \tilde{P}(f) \right|^2$$

we may rewrite Eq. (23) as

$$A_{RP} = \frac{\int_{-\infty}^{\infty} \left| \tilde{R}(f) \right|^2 \left| \tilde{P}(f) \right|^2 df}{\left[\int_{-\infty}^{\infty} \left| \tilde{R}(f) \right|^4 df \int_{-\infty}^{\infty} \left| \tilde{P}(f) \right|^4 df \right]^{1/2}} . \quad \textbf{(25)}$$

Note that this quantity is real.

In practice, the $\tau = 0$ component of the autocorrelation function is very large and the function defined by Eq. (25) always generates a misleading good "match". In order to focus the influence on the matching of non-zero lag values, and to remove most of the influence of the noise (assumed uncorrelated to the signal), the $\tau = 0$ component is removed before forming the autocorrelation match. This is equivalent to removing the mean from the frequency-domain squared amplitudes, i.e.,

$$A_{RP} = \frac{\int_{-\infty}^{\infty} \left| \tilde{R}'(f) \right|^2 \left| \tilde{P}'(f) \right|^2 df}{\left[\int_{-\infty}^{\infty} \left| \tilde{R}'(f) \right|^4 df \int_{-\infty}^{\infty} \left| \tilde{P}'(f) \right|^4 df \right]^{1/2}} , \quad \textbf{(26)}$$

where the primed quantities are defined by removing the mean of the square,

$$\left| \tilde{R}'(f) \right|^2 = \left| \tilde{R}(f) \right|^2 - \left\langle \left| \tilde{R}(f) \right|^2 \right\rangle_f , \left| \tilde{P}'(f) \right|^2 = \left| \tilde{P}(f) \right|^2 - \left\langle \left| \tilde{P}(f) \right|^2 \right\rangle_f , \quad \textbf{(27)}$$

and $\langle \ \rangle_f$ indicates an average over all frequencies. Thus, it is possible for A_{RP} to become negative. Equation (26) then defines the time-domain autocorrelation matching (TACM) algorithm.

Previous investigations using the TACM algorithm (de Kooter, 1997) found that the footprint size was very small (~ wavelength), and small, relative travel time errors (due to

variety of mismatch phenomena) result in large phase errors at high frequency. Thus, TACM seemed useful only for very low frequency signals. However, it was observed that while TACM might produce poor matches at correct source locations, the time-domain amplitude-squared signals seemed quite similar. Therefore, matching $|R(t)|^2$ with $|P(t)|^2$ might prove to be more robust.

B. FREQUENCY-DOMAIN AUTOCORRELATION MATCHING (FACM)

Matching the time-domain squared amplitude signals is equivalent to forming the ambiguity function

$$\tilde{A}_{RP} = \frac{\int_{-\infty}^{\infty} |R(t)|^2 |P(t)|^2 dt}{\left[\int_{-\infty}^{\infty} \left| R(t) \right|^4 dt \int_{-\infty}^{\infty} \left| P(t) \right|^4 dt \right]^{1/2}}. \tag{28}$$

However, based on the previous derivations, this can be defined as a matching of the frequency-domain autocorrelation functions,

$$\tilde{A}_{RP} = \frac{\int_{-\infty}^{\infty} \tilde{C}^*_{\tilde{R}\tilde{R}}(\phi) \tilde{C}_{\tilde{P}\tilde{P}}(\phi) d\phi}{\left[\int_{-\infty}^{\infty} \left| \tilde{C}_{\tilde{R}\tilde{R}}(\phi) \right|^2 d\phi \int_{-\infty}^{\infty} \left| \tilde{C}_{\tilde{P}\tilde{P}}(\phi) \right|^2 d\phi \right]^{1/2}}, \tag{29}$$

where

$$\tilde{C}_{\tilde{P}\tilde{P}}(\phi) = \frac{F^{-1}\left[|P(t)|^2 \right]}{\int_{-\infty}^{\infty} |P(t)|^2 dt} \text{ and } \tilde{C}_{\tilde{R}\tilde{R}}(\phi) = \frac{F^{-1}\left[|R(t)|^2 \right]}{\int_{-\infty}^{\infty} |R(t)|^2 dt}. \tag{30}$$

Note that the Fourier-Transform convention used here is chosen in order to be consistent with the model calculations as described in Eq.(13) (Press, et al., 1988).

As before, we seek to reduce the overwhelming effect of the zero-lag $(\phi = 0)$ component by removing the mean of the squared amplitude of the time-domain signal. The actual form of the FACM algorithm to be implemented is then defined by

$$\tilde{A}_{RP} = \frac{\int_{-\infty}^{\infty} |R'(t)|^2 |P'(t)|^2 dt}{\left[\int_{-\infty}^{\infty} |R'(t)|^4 dt \int_{-\infty}^{\infty} |P'(t)|^4 dt \right]^{1/2}}, \tag{31}$$

where

$$|R'(t)|^2 = |R(t)|^2 - \left\langle |R(t)|^2 \right\rangle_t, |P(t)|^2 = |P'(t)|^2 - \left\langle |P(t)|^2 \right\rangle_t, \tag{32}$$

and $\langle \ \rangle_t$ indicates an average over all times. Thus, it is also possible for $\tilde{A}_{RP}$ to become negative.

While Eq. (31) is formally valid, there is an inherent ambiguity in the absolute times. In the TACM method, only relative times were used but absolute frequency was important. Neglecting Doppler influences, there is no ambiguity with frequency. In the FACM method, however, we must search over time for an optimal match. Thus, we re-define our FACM function as

$$\tilde{A}_{RP} = \max_{\tau} \left\{ \frac{\int_{-\infty}^{\infty} |R'(t+\tau)|^2 |P'(t)|^2 dt}{\left[\int_{-\infty}^{\infty} |R'(t)|^4 dt \int_{-\infty}^{\infty} |P'(t)|^4 dt \right]^{1/2}} \right\}, \tag{33}$$

where $\max_{\tau}$ represents the maximum value of the function for any value of the search parameter τ. Therefore, by sliding the replica signal in time, we search for the best match. While the introduction of this new search parameter does increase the computational load of the algorithm somewhat, it might also have the benefit of increasing the size of the footprint since it may be expected that signals measured at nearby points in space decorrelate more rapidly in time (when no sliding is performed) than the structural character of the overall arrival pattern.

C. LOGARITHMIC AUTOCORRELATION MATCHING (LTACM & LFACM)

It has recently been shown that matching logarithms of functions may be optimal for certain types of signals in certain environments (Makris, 1996). In addition, it was suggested that matching the logarithms would naturally enhance the significance of later, weaker arrivals. Therefore, in addition to the TACM and FACM ambiguity functions defined previously, we will also investigate the structure of the ambiguity surfaces defined by

$$B_{RP} = \frac{\int_{-\infty}^{\infty} \left(\log\left|C_{RR}(\tau)\right|\right)\left(\log\left|C_{PP}(\tau)\right|\right) d\tau}{\left[\int_{-\infty}^{\infty} \left(\log\left|C_{RR}(\tau)\right|\right)^2 d\tau \int_{-\infty}^{\infty} \left(\log\left|C_{PP}(\tau)\right|\right)^2 d\tau\right]^{1/2}} \quad \text{(LTACM)} \qquad \textbf{(34)}$$

and

$$\tilde{B}_{RP} = \frac{\int_{-\infty}^{\infty} \left(\log\left|\tilde{C}_{\tilde{R}\tilde{R}}(\phi)\right|\right)\left(\log\left|\tilde{C}_{\tilde{P}\tilde{P}}(\phi)\right|\right) d\phi}{\left[\int_{-\infty}^{\infty} \left(\log\left|\tilde{C}_{\tilde{R}\tilde{R}}(\phi)\right|\right)^2 d\phi \int_{-\infty}^{\infty} \left(\log\left|\tilde{C}_{\tilde{P}\tilde{P}}(\phi)\right|\right)^2 d\phi\right]^{1/2}} \quad \text{(LFACM)}. \qquad \textbf{(35)}$$

Note that there is now no simple relationship between these functions and their corresponding transform-domain functions.

IV. EXPERIMENTAL SETUP AND RESULTS

To gain insight into the performance of the autocorrelation matching algorithms, several numerical experiments were conducted. The experiments have primarily been performed for the frequency band from 500 Hz to 2300 Hz. The baseline for the results was defined as the results of the autocorrelation matching of a PE generated source and PE generated templates. For most of the experiments the source range was varied between 1000 m and 10 km, the source depth varied between 10 m and 100 m. Received signals downrange were numerically extracted at depths corresponding to two short aperture arrays spanning 19.43 m to 22.36 m and 54.79 m to 57.71 m. All ambiguity surfaces generated in this work are based on signals received at central elements of these arrays, either 21 m (shallow receiver) or 56.3 m (deep receiver). The generation of the ambiguity surfaces was performed using Matlab routines (Mathworks Inc., 1996). For the environments defined below, the first arrivals at this range arrive at approximately 0.8 to 7 seconds after the transmission and the significant part of the arrival structure is about 0.4 seconds in length. The signals and replicas used were 2048 points in length which for a bandwidth of 1800 Hz corresponds to a frequency spacing of 0.878906 Hz. As the project did not focus on the frequency characteristics of the source function, the same Gaussian spectral shape has been assumed for the source signal and the templates. In all presentations, the absolute scale of the pressure field calculation has been neglected since this drops out of the normalized ambiguity functions.

Note that some plots of ambiguity surfaces displayed in this thesis are difficult to interpret in terms of the actual peak locations relative to the displays using a color monitor. The degradation is due to the limited size and print quality of the plots.

A. ENVIRONMENTS

For the synthetic experiments, seven shallow water environments, including both range-independent and range-dependent, were defined. Typical environmental profiles for the seven cases are illustrated in Figs. IV.A.1 (a-e). The synthetic signals that were used as the original signals for the creation of the ambiguity surfaces were generated with varying random uncertainties in the environmental parameters of the different scenarios. The dashed lines in Figs. IV.A.1 (b-e) indicate the corresponding standard deviations. However, when generating the replica signals for matching, only range-independent estimates of the average environment were employed.

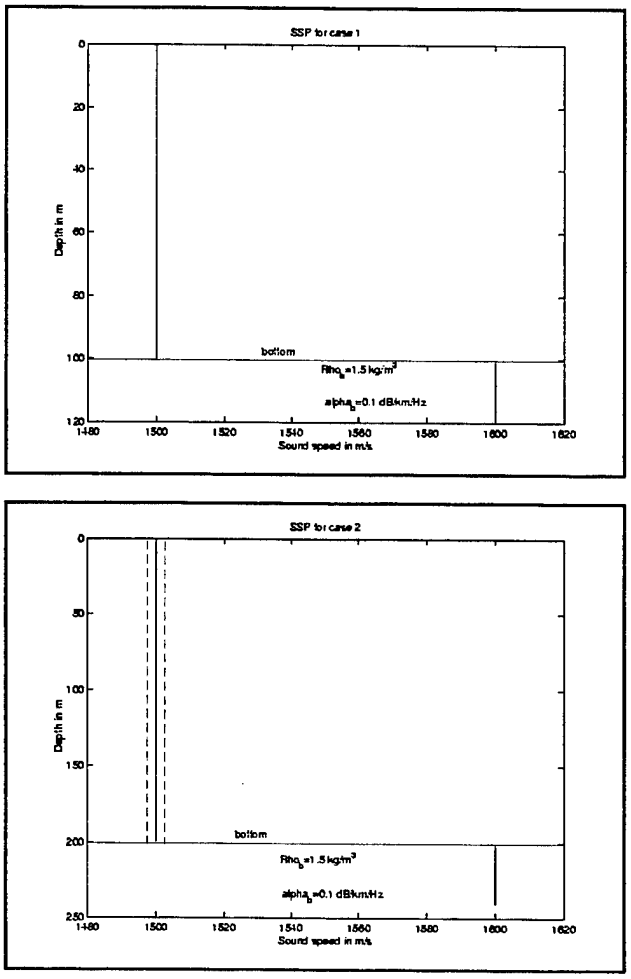

(a)

(b)

Figure IV.A.1: Sound speed profiles for synthetic environments (a) Case 1 and (b) Case 2

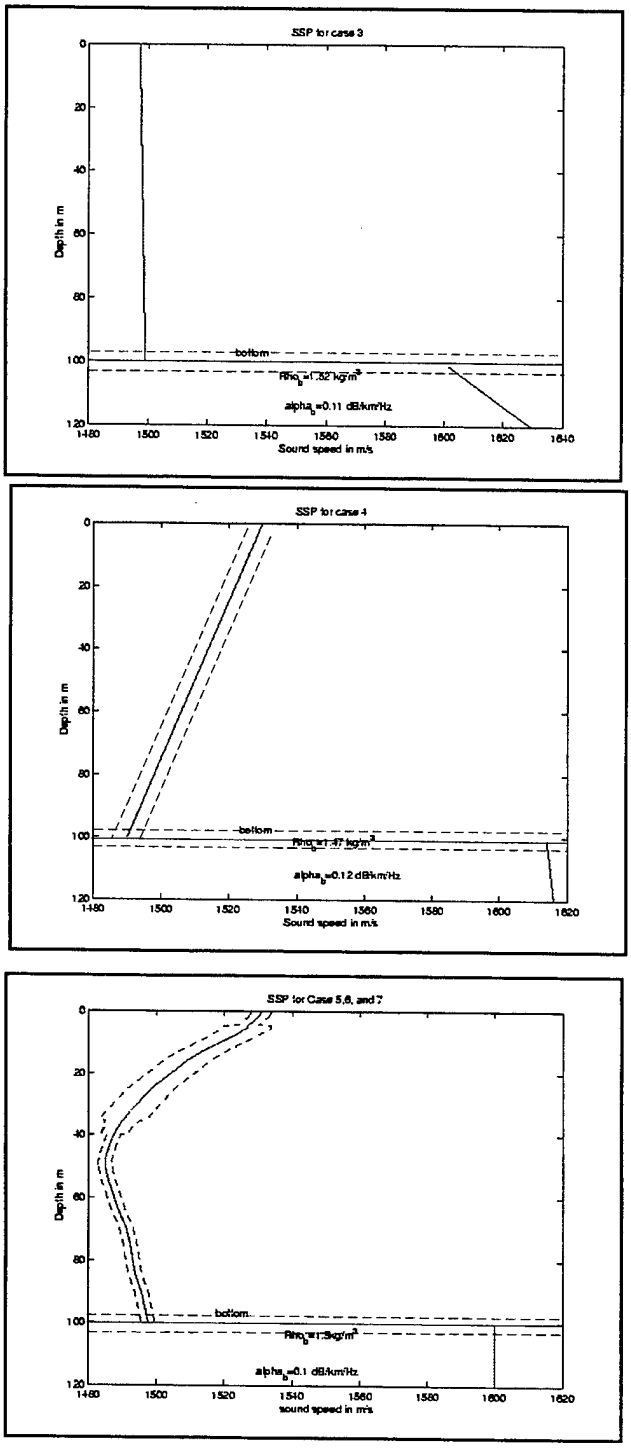

(c)

(d)

(e)

Figure IV.A.1 (continued): Sound speed profiles for synthetic environments (c) Case 3,(d) Case 4, and (e) Cases 5-7 from SWARM experiment (Apel et al., 1997)

The typical parameter values used to define the bottom were a density of ϱ_b= 1.5 g/cm^3 and an attenuation of α_b= 0.10 dB/km/Hz. The water was always assumed to have a density of 1.0 g/cm^3. In addition to the third case mentioned above, an environment with the same parameters but with a slightly altered sound speed profile (SSP) was generated. For the fourth environment, replicas have been made with an average in both the SSP and the bathymetry, with an average in the SSP only, with an average in the bathymetry only, and with all parameters known exactly. Replicas have also been made for the first environment with a different bottom bathymetry assuming c_b =1575m/s with a gradient of 1.5 (m/s)/m in contrast to the bottom parameters mentioned above.

Case 1 is the only scenario where the environment was both range-independent and exactly known. In all other cases, environmental uncertainties were introduced. Cases 5 through 7 have a similar environment defined by a field of nonlinear internal solitons of varying extent within the water column. The differences between these cases were due to the placement of the source and receiver within the soliton field. The variability of sound speed due to the presence of these solitons is indicated in Fig. IV.A.1.(e). The respective uncertainties introduced for the different cases will be stated in detail in the next section together with the discussion of the results for the different matching algorithms.

For each of the seven scenarios above, four different source locations and two different receiver locations were chosen. The bottom bathymetry was treated as range-independent for the generation of all replica templates although some minor bathymetry fluctuations were used in the generation of the original synthetic signal for most cases.

B.1. Case 1: Isospeed sound speed profile, 100 m deep

In this case the environment was exactly the same for the generation of the replica signal and the synthetically generated measured signal. Synthetic data for four different source

locations between 2.6 km and 9.9 km in range and 18 m to 83 m in depth were investigated at receiver depths of 21 m and 56.3 m. An analysis of the correlation between propagation loss and pulse spread of the received signal with respect to the "goodness" of a localization did not provide any meaningful results. The maximum spatial cross-correlation of the frequency-domain autocorrelation functions of the signals across the shallow array as seen in Fig. IV.B.1(a), however, shows that for this scenario there are distinct differences between these functions at different depths even though the corresponding receivers were only seperated by about 20 cm. This high spatial decorrelation may infer a higher probability of a good, less ambiguous localization since each array element receives a unique arrival structure.

For all four source locations and both receiver depths, distinct localizations could be made at the correct source positions. Some results are shown in Figs. IV.B.1 (b-f). The TACM method provided a larger footprint size when only the low frequencies, i.e. the first quarter (500-950 Hz), of the total bandwidth (500-2300 Hz) were considered as displayed in Figs. IV.B.1.(b) and (c). The footprint size is measured as the area adjacent to the location of the peak value in which the corresponding values on the ambiguity surface equal at least half the peak value. When all frequencies were used, the footprint was roughly 3.5 m x 25 m as compared to a footprint of nearly 4.5 m x 55 m when using only the first quarter of the bandwidth. This is consistent with previous work (de Kooter, 1997) which showed that TACM is highly sensitive to phase mismatch at high frequencies.

For the FACM method, the use of only the lower or higher frequencies of the total bandwidth affected the results negatively providing a smaller footprint size and higher sidelobe levels. The FACM method produced basically identical results when only every fourth data point was sampled of the full bandwidth. This is to be expected, however, since the frequency sampling was roughly four times smaller than needed to avoid aliasing or wrap-around in the time domain. The FACM generally provided a larger footprint size than the TACM, roughly 5 m x 80 m. This was especially obvious when the search grid was drastically undersampled spatially. The best spatial sampling would be provided by using a grid spacing of about one half of the minimum wavelength present. For a sound speed of 1500 m/s and a maximum frequency of 2300 Hz, we find the best spatial sampling at 0.3261 m. Thus all scenarios that were analyzed were spatially undersampled, some extremely but

others only slightly.

The FACM always provided the larger peak values as compared to the TACM. The peak-to-sidelobe levels, however, were high (> 4 dB) for all localizations for both algorithms even when the environment was spatially undersampled. The location of the receiver did not have any significant effect on the results. They were almost identical for both shallow and deep receiver locations.

Changing the sound speed in the bottom to a higher value and using a different bottom sound speed gradient for the generation of the measured signals did almost not affect the results at all. For all four source locations and both receiver depths, distinct localizations could be made at correct source positions using both algorithms with the same footprint-size and peak-to-sidelobe levels as before.

(a)

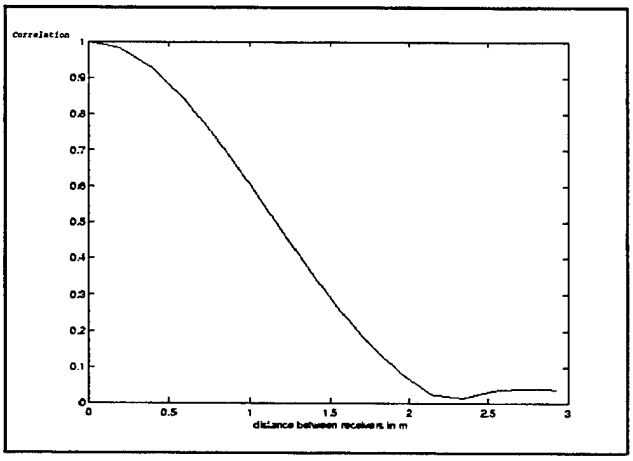

Figure IV.B.1: (a) Maximum spatial correlation of the frequency-domain autocorrelation functions across the shallow array at 5.3 km.

(b)

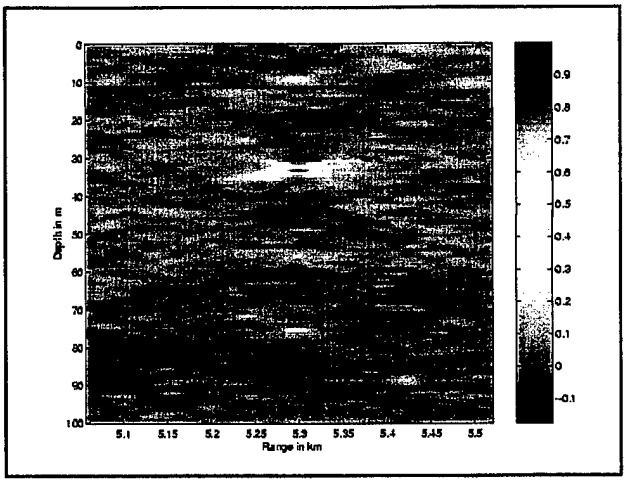

(c)

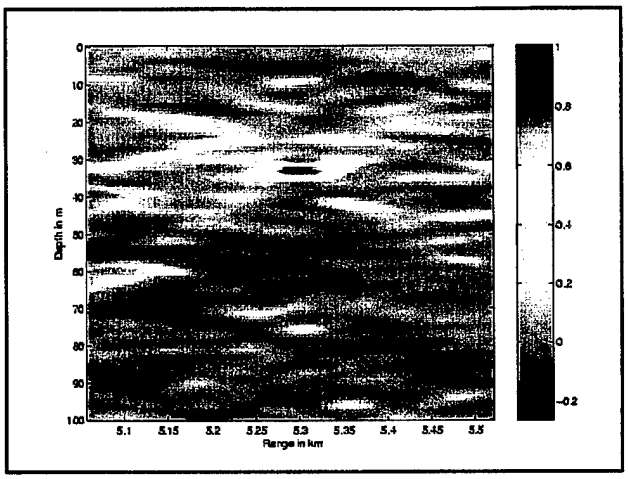

Figure IV.B.1 (continued): TACM for Case 1. (b) Ambiguity surface for a shallow receiver localizing to a source location at 5.3 km, 33 m deep. Spatial sampling 128 points in depth and 150 points in range. All 2048 data points are used.(c) Ambiguity surface for shallow receiver localizing to a source location at 5.3 km, 33 m deep. Spatial sampling 128X150. Only first 512 data points are used (bandwidth 500-950Hz).

(d)

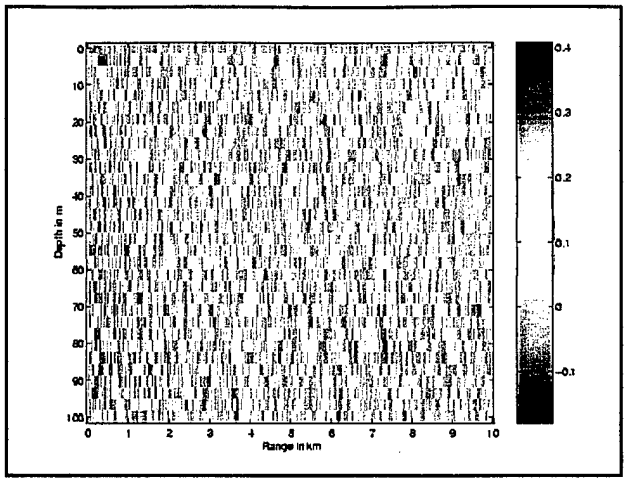

Figure IV.B.1 (continued): TACM for Case 1. (d) Ambiguity surface for deep receiver localizing to a source location at 7.3 km, 61 m deep. Spatial sampling 32X300. All 2048 data points are used.

(e)

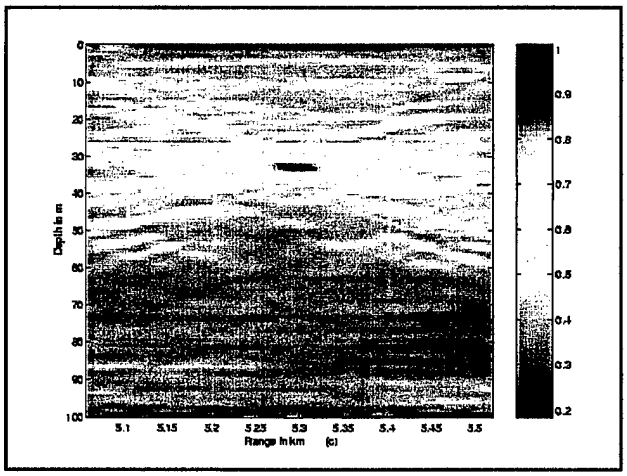

Figure IV.B.1 (continued): FACM for Case 1-(e) Ambiguity surface for shallow receiver localizing to a source location at 5.3 km, 33 m deep. Spatial sampling 128X150. 512 data points are used (full bandwidth).

(f)

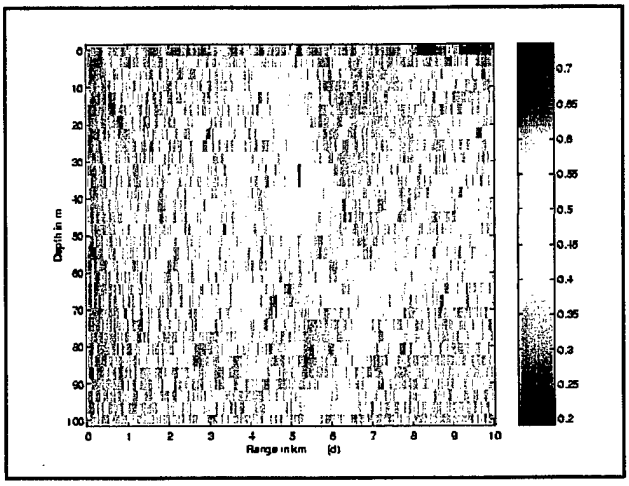

Figure IV.B.1 (continued): FACM for Case 1. (f) Ambiguity surface for shallow receiver localizing to a source location at 5.3km, 33 m deep with mismatch in bottom parameters. Spatial sampling 32X300. 512 data points are used (full bandwidth).

B.2. Case 2: Isospeed sound speed profile, 200 m deep

As in Case 1 four different source locations with both receiver depths were analyzed. In this case however, a slight environmental mismatch was introduced. Instead of a strictly isospeed SSP, an uncertainty of (+/- 3 m/s) in the SSP was applied to a few depth points in the SSP for the generation of the synthetic measured signals. The replicas were then generated using only an average or approximate SSP. Correct localizations could be made in all cases using both algorithms and both receiver depths even when the environment was spatially undersampled. The results are comparable to those found for Case 1. However, a slight decrease in the peak-to-sidelobe levels was observed compared to Case 1, more so for the TACM (3 dB) than for the FACM (4 dB). The maximum values also decreased as compared to Case 1 which was expected because of the environmental uncertainty. The footprint size for the FACM remained almost

unchanged compared to Case 1 whereas it decreased for the TACM to approximately 3.5 m x 45 m. Again, the FACM proved to be more robust than the TACM to spatial undersampling and environmental mismatch. As in Case 1 the location of the receiver did not significantly affect the results. The spatial correlation of the frequency domain autocorrelation functions was comparable to Case 1.

B.3. Case 3: Positive sound speed gradient

Again four different source locations with both receiver depths were analyzed. In this case, an uncertainty in the bottom bathymetry was introduced. Specifically, the depth was varied by (+/- 3 m) with range from the original 100 m for the generation of the measured signal. A further decrease in the peak-to-sidelobe levels was observed for both the FACM and TACM as compared to Case 2. The footprint size for the FACM did not change much compared to Case 2, as seen in Fig. IV.B.3(d), while it decreased further for the TACM to 3 m x 35 m, as displayed in Fig. IV.B.3(b). Correct localizations, however, could still be made in all cases with both algorithms despite undersampling spatially.

When a mismatch in the sound speed profile was introduced instead of the uncertainty in the bathymetry, the results did not change significantly with respect to the shallow receiver. However, the localization with the deep receiver became much poorer for both algorithms. The peak-to-sidelobe levels decreased drastically to approximately 1 dB for the TACM and 2 dB for the FACM while the footprint size decreased to 3 m x 30 m for the TACM and 6 m x 64 m for the FACM as seen in Figs. IV.B.3(c) and (e). The worst results occured when both source and receiver were at a deep location. This can be explained by the fact that in this environment the acoustic rays are bent upwards so that at a distant deep receiver the pressure field is more ambiguous due to fewer arrivals with respect to the possible source location. Localizations, however, were still made even when the search grid was spatially undersampled.

For both algorithms, the mismatch in the SSP had a stronger effect on the results than the

mismatch introduced in the bathymetry. Overall the FACM proved to be more consistent for the same source locations than the TACM. It can be stated that an environmental mismatch in more complex SSP scenarios (as in Case 3) affects the results more than the same uncertainty in a less complex scenario (as in Case 2).

The maximum spatial cross-correlation of the frequency-domain autocorrelation functions across the shallow array, as seen in Fig. IV.B.3(a), illustrates a slight increase in the correlation of the signals as compared to Case 1 and Case 2. This is consistent with the observed increasing ambiguity (i.e., lower peak-to-sidelobe levels) for the localization process. Thus, the higher the spatial correlation, the more difficult it becomes to determine the true source localization.

(a)

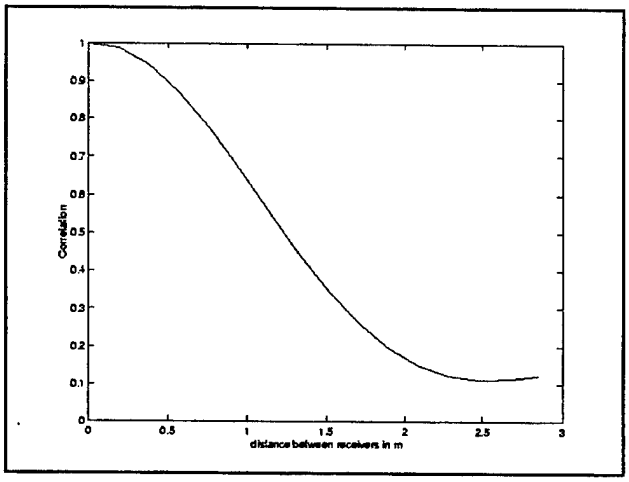

Figure IV.B.3: (a) Spatial correlation of the frequency-domain autocorrelation functions across the shallow array at 7.2 km.

(b)

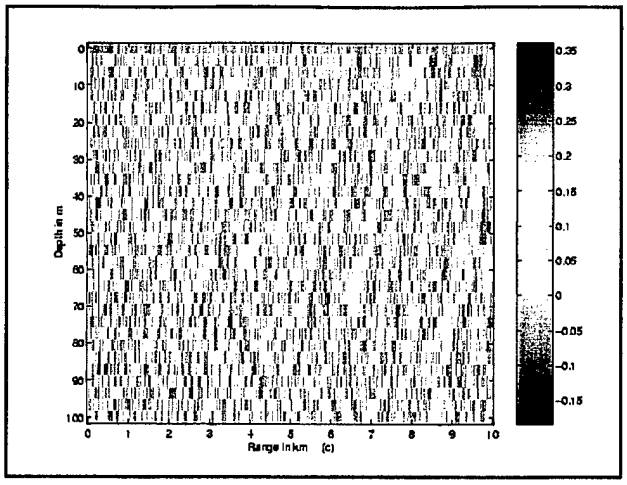

Figure IV.B.3 (continued): TACM with mismatch in only the bathymetry. (b) Ambiguity surface for a deep receiver localizing to a source location at 9.3 km, 59 m deep. Spatial sampling 32X300. All 2048 data points are used.

(c)

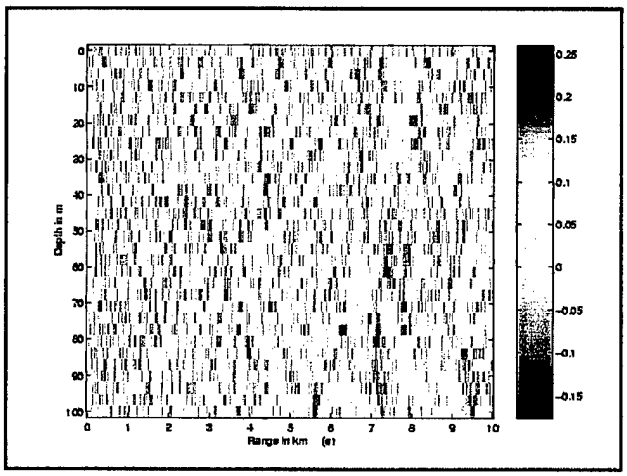

Figure IV.B.3 (continued): TACM for Case 3 with mismatch in sound speed profile only. (c) Ambiguity surface for a deep receiver localizing to a source location at 7.2 km, 53 m deep. Spatial sampling 32X300. All 2048 data points are used.

(d)

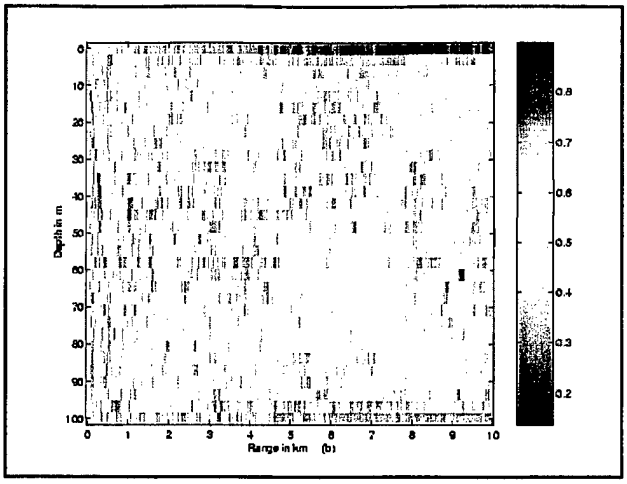

Figure IV.B.3 (continued): FACM for Case 3 with mismatch in bathymetry only.(d) Ambiguity surface for deep receiver localizing to a source location at 9.3 km, 59 m deep. Spatial sampling 32X300. Only 512 data points are used (full bandwidth).

(e)

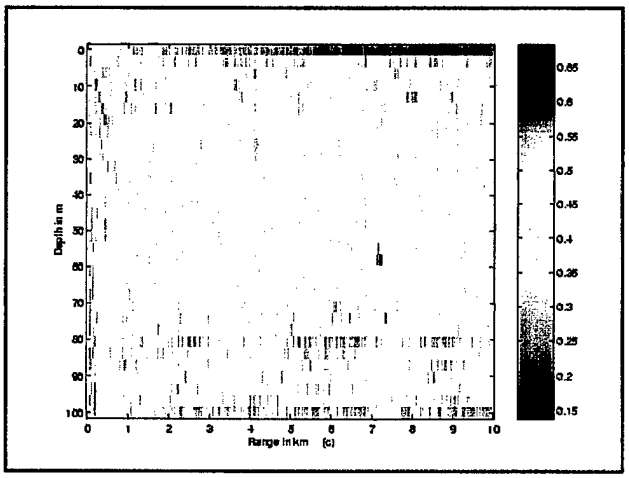

Figure IV.B.3 (continued): FACM for Case 3 with mismatch in SSP only. (e) Ambiguity surface for deep receiver localizing to a source location at 7.2 km, 53 m deep. Spatial sampling 32X300. 512 data points are used (full bandwidth).

B.4. Case 4: Strong negative gradient in SSP

Again four different source locations were analyzed for both receiver depths and both algorithms, FACM and TACM. In additon to a fairly high uncertainty in the sound speed profile, an uncertainty in the bathymetry was introduced. For the TACM, correct localizations could only be made when the search grid was spatially well sampled. Even then the peak had to be enhanced by raising all values for the ambiguity surface to a higher power to make it distinctively visible in the plot (equivalent to re-defining the color palette to enhance lower values) as seen in Fig. IV.B.4(b). There was no significant improvement observed in the results for the TACM when considering only the low frequency band or the full bandwidth due to the very strong environmental mismatch.

For the FACM, localizations could be made in most cases despite a rather poor footprint size of 3 m x 32 m and low peak-to-sidelobe levels around 1 dB as seen in Fig. IV.B.4(d). This was true also for the strongly spatially undersampled search grid. Sampling only every fourth point of the given bandwidth produced the same results as compared to sampling all points, as before.

A technique that seemed to provide improved results for the FACM was zero-padding the signal in the frequency-domain to twice its length. By doing this, the time-domain spacing is reduced to half and therefore additional data points, i.e. a better time resolution, is provided (Ziomek, 1995). Thus, the probability of a correct localization by sliding the time window over twice as many data points increases. Of course, this provides no true additional information. But since increments in time are closely related to increments in range for such propagation problems, the influence of this zero-padding technique is similar to an increased spatial resolution which the FACM algorithm takes advantage of by searching for the maximum match when sliding the time-domain signal. Additional zero-padding would not be expected to continually improve the results, and so was not considered further. Also, the computational effort increases when zero-padding a signal before matching it with the replicas.

Isolating the uncertainties, i.e. considering a mismatch in the sound speed profile only with no mismatch in bathymetry and then vice versa, showed for both algorithms that a mismatch

in the sound speed profile is much more devastating to the localization results than a mismatch in the bathymetry. The worst results occured when both types of mismatch were introduced. In most cases, the FACM proved again to be more robust and capable of providing better results than the TACM as displayed in Figs. IV.B.4(b) and (d). However, for many cases with a mismatch in only the SSP, no localization could be made using either algorithm. The ambiguity surface showed too many false matches with values close to one, so that a distinction between peak and sidelobes could no longer successfully or correctly be made. For both algorithms, the results improved considerably with improved spatial sampling as seen in Figs. IV.B.4(c),(e). It is obvious that when the environmental mismatch increases the spatial sampling becomes more important and needs to be increased in order to provide good results.

Generally, the very strong negative gradient in the soundspeed profile and the resulting strong downward bending of the acoustic energy makes a localization extremely difficult. The maximum spatial cross-correlation of the frequency-domain autocorrelation functions across the deep array, as seen in Fig. IV.B.4(a), shows a rather poor decorrelation (relatively high correlation) between these quantities at the corresponding receiver locations, which infers an even more difficult, i.e. more ambiguous, localization process as compared to Case 3.

(a)

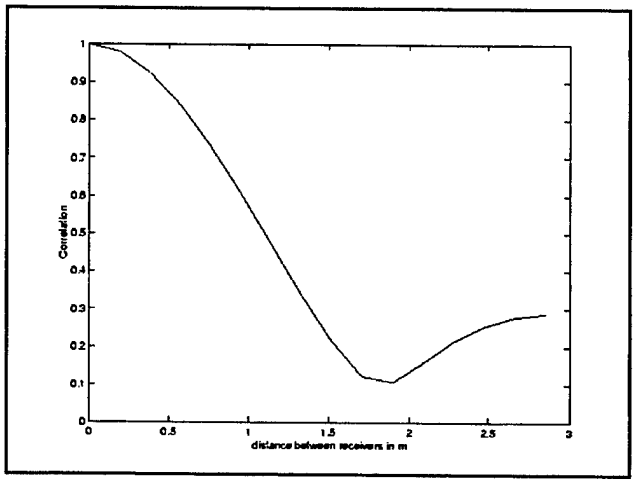

Figure IV.B.4 (a): Spatial cross-correlation of the frequency-domain autocorrelation functions across the deep array at 7.2 km.

(b)

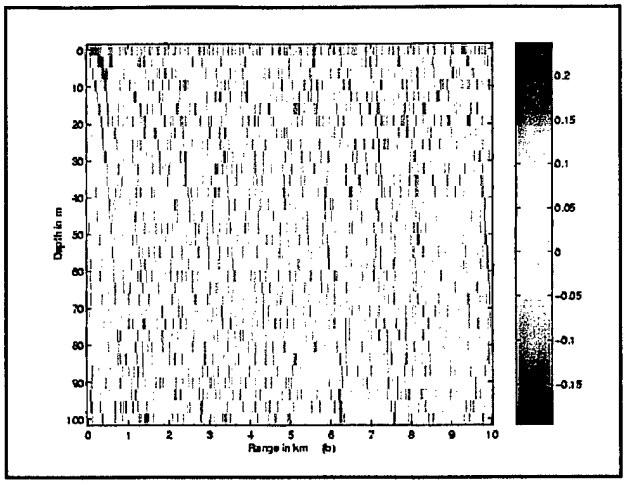

Figure IV.B.4 (continued): TACM for Case 4. (b) Ambiguity surface for shallow receiver localizing to a source location at 7.2 km, 18 m deep. Spatial sampling 32X300. All 2048 data points are used. No match.

(c)

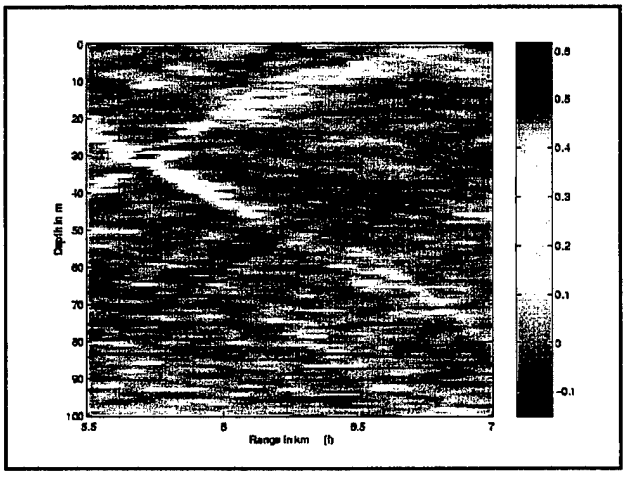

Figure IV.B.4 (continued): TACM for Case 4 with mismatch in sound speed profile and bathymetry. (c) Ambiguity surface for shallow receiver localizing to a source location at 5.7 km, 31 m deep. Spatial sampling 128X150. All 2048 data points are used.

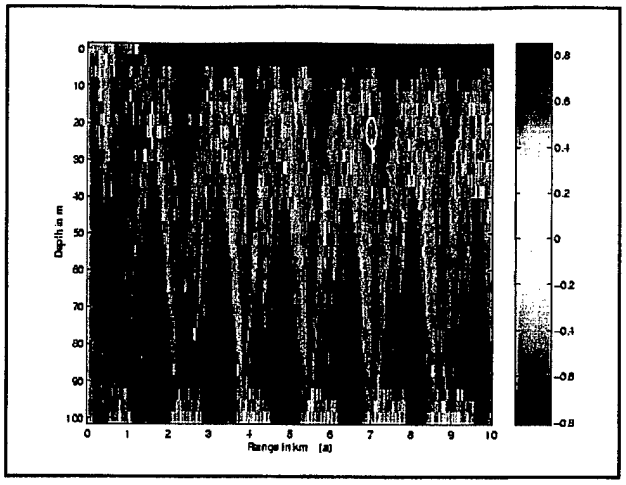

(d)

Figure IV.B.4 (continued): FACM for Case 4 with mismatch in SSP and bathymetry. (d) Ambiguity surface for shallow receiver localizing to a source location at 7.2 km, 18 m deep. Spatial sampling 32X300. 512 data-points used. Values raised to the fifth power.

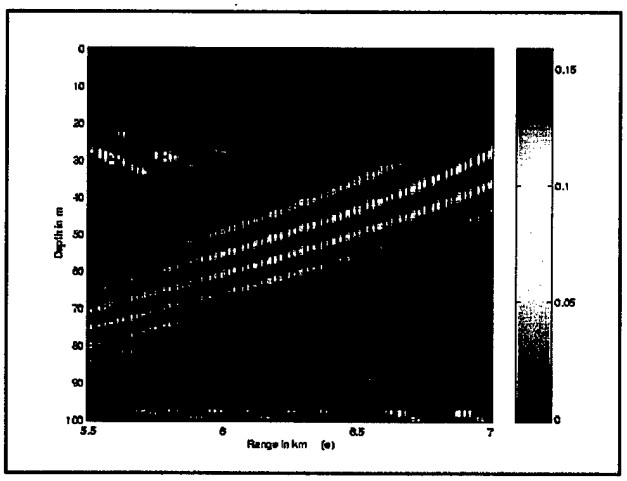

(e)

Figure IV.B.4 (continued): FACM or Case 4. (e) Ambiguity surface for shallow receiver localizing to a source location at 5.7 km, 31 m deep. Spatial sampling 128X150. Every fourth data point is used. Mismatch in SSP and bathymetry. Values raised to fifth power.

B.5. Case 5: Realistic, slightly range-dependent environment

For the generation of the synthetic measured signals in this case, a moderately range-dependent bathymetry similar to that of Case 3 was used. In addition, the sound speed structure in the water column was extracted from a real experimental database provided by Chiu (Chiu et al., 1997). This data was taken from a shallow water experiment and includes the influence of a nonlinear internal soliton wave packet which can significantly perturb the sound speed structure, as seen in Fig. IV.B.5(a). The sound speed information (in m/s) is given by the color coding. For this case, the sound speed profiles were extracted between 25 km and 35 km of this database. The result is a slightly range-dependent SSP with no major perturbations due to the soliton packets. For the generation of the synthetic data sets, the position in range of the receiving arrays was assumed fixed while the various source locations were changed in range and depth. For the generation of the replicas, only an average bottom depth and average SSP were used to produce a range-independent environment. Thus, mismatch existed in bathymetry and sound speed, and the "real" environment was range-dependent in both while the replicas assume an approximate range-independent scenario.

Despite these uncertainties and a rather poor spatial decorrelation of the frequency-domain autocorrelation functions at the receivers as displayed in Fig. IV.B.5(b), the results for both algorithms, TACM and FACM, were similar as seen in Figs. IV.B.5(c)-(f). However, the relative position of source and receiver proved to be important for the localization. Specifically, due to the presence of a sound channel, the similar location of either both source and deep receiver in the channel or both source and shallow receiver above the channel provided good localizations. On the other hand, in cases where only either source or receiver were put into the SOFAR channel the results were poor. No significant differences between the localizations made using FACM and TACM were observed apart from a better footprint size for the FACM (6 m x 64 m) as compared to the TACM (3 m x 32 m). The peak-to-sidelobe levels were approximately 2 dB for both algorithms.

(a)

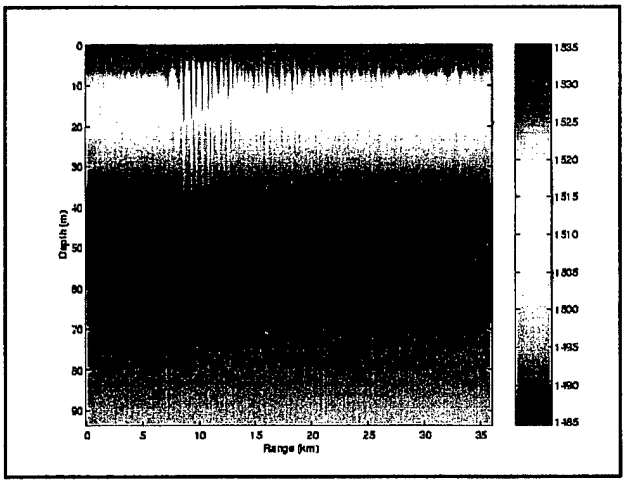

Figure IV.B.5: (a) Soliton field between approximately 5 and 30 m depth and 5 and 20 km range

(b)

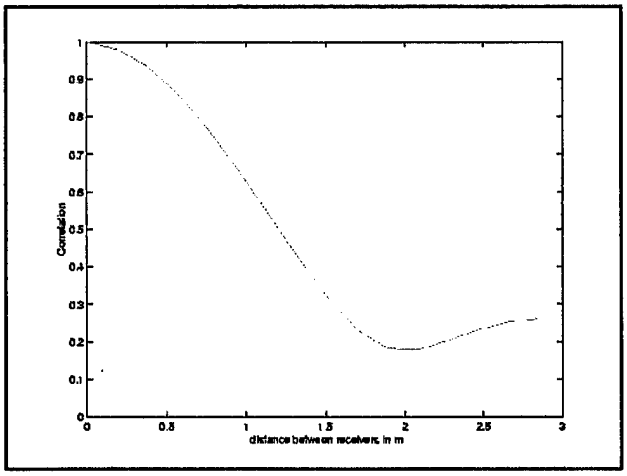

Figure IV.B.5 (continued): (b) Spatial cross-correlation of the frequency-domain autocorrelation functions across the deep array at 4.4 km.

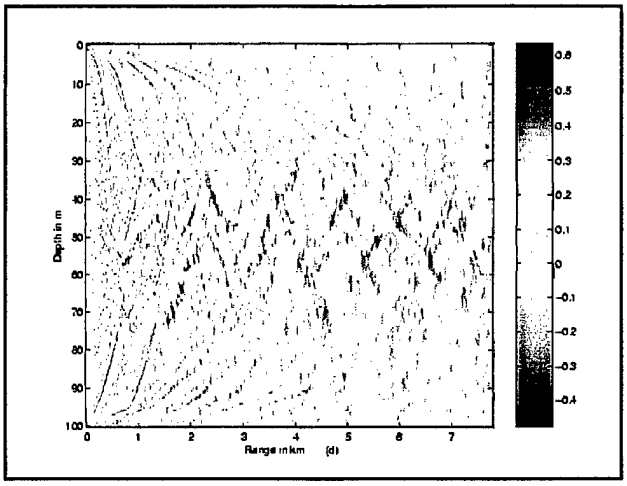

(c)

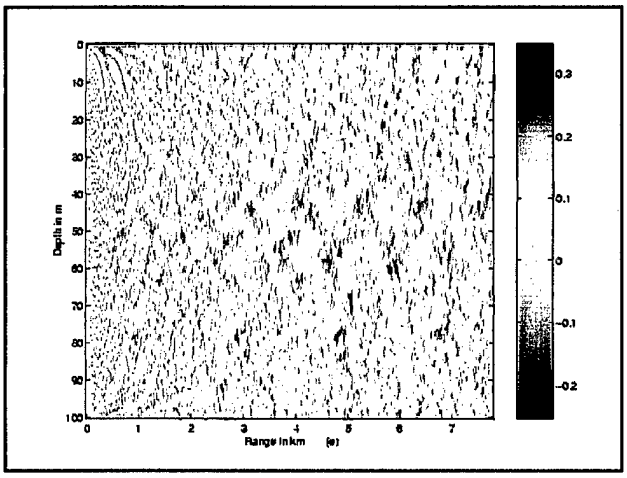

(d)

Figure IV.B.5 (continued): TACM for Case 5 with mismatch in sound speed profile (range dependence). (c) Ambiguity surface for deep receiver localizing to a source location at 5.9 km, 51 m deep. Spatial sampling 171X500. All 2048 data points are used. (d) Ambiguity surface for a deep receiver localizing to a source location at 7.2km, 32m deep (just within sound channel). Spatial sampling 171X500. All 2048 data points are used.

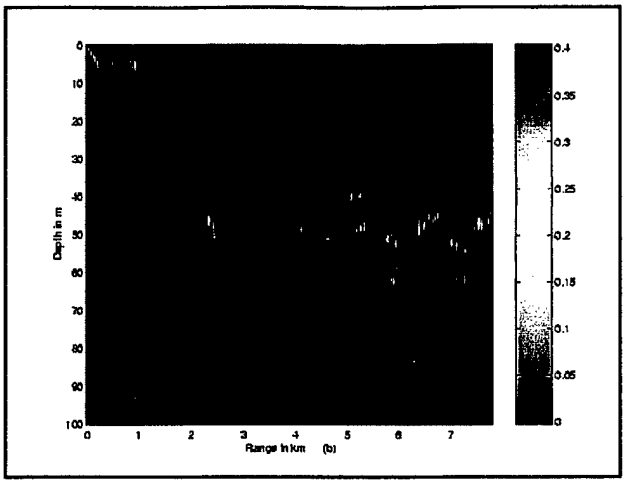

(e)

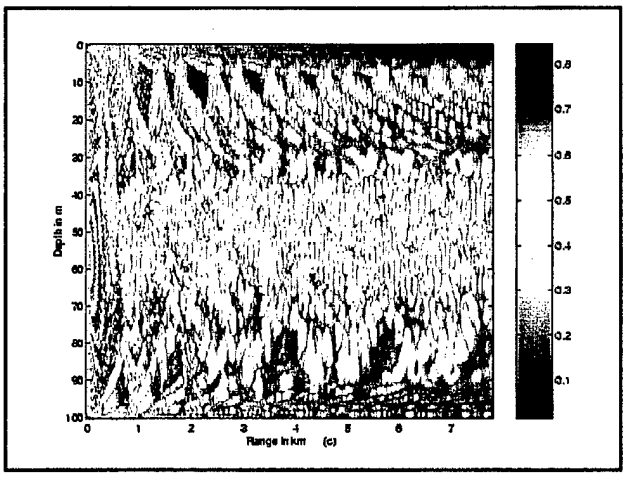

(f)

Figure IV.B.5 (continued): FACM for Case 5. (e) Ambiguity surface for deep receiver localizing to a source location at 5.9 km, 51 m deep. Spatial sampling 171X500. 512 data points are used. (f) Ambiguity surface for deep receiver localizing to a for source location at 7.2 km, 32 m deep. Spatial sampling 171X500. Every fourth data point is used (full bandwidth).

B.6. Case 6: Range-dependent SSP pertubed by internal wave soliton field from 7.5 km outward

For the generation of the synthetic signals in this case, the SSP was made much more range-dependent by extracting from the experimental data set between ranges 0 km and 10 km (refer to Fig. IV.B.5(a)). This produced an environment perturbed by the soliton packet from about 7.5 km outward from the receiver array. As before, the environment was assumed fixed relative to the receiver position while the various source locations were moved about such that the source may lie within the range of soliton influence. Again, a single, average SSP and bottom depth were used in the generation of the replicas.

In this case, the peak-to-sidelobe levels were a little lower for both algorithms (1 dB) as compared to Case 5 for all source locations including those closer than the soliton field. For those source locations closer than the soliton field, this is presumably due to the influence of the solitons on the average, range-independent SSP. For the source locations within the range of the soliton field the localization was excellent for both source and receiver in the channel using both FACM and TACM. Again, the footprint-size for the FACM was larger than for the TACM and approximately the same as in Case 5 as displayed in Figs. IV.B.6(a),(c),(d),(f). For the shallow receiver, however, no localization was made for the TACM whereas the FACM provided a rather poor but correct localization as seen in Figs. IV.B.6(b) and (e). Therefore, the FACM continues to be more robust against environmental mismatches than the TACM, being able to make correct localizations when the TACM fails.

The presence of the SOFAR channel represents a rather favorable SSP for good localizations, and thus the environmental mismatches introduced can be larger than those in Case 4 and still provide correct localizations. The cross-correlation between the frequency-domain autocorrelation functions of the receivers of the deep array are effectively the same as for Case 5, suggesting that little or no energy from the synthetic source locations interacted with the soliton field. The same comments then apply.

(a)

(b)

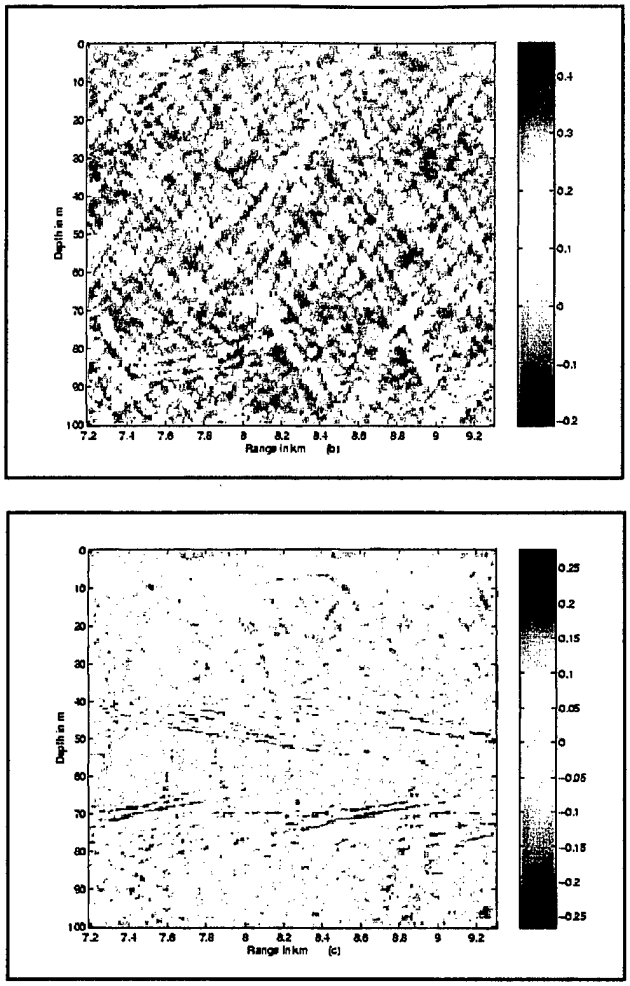

Figure IV.B.6: TACM for Case 6 with range dependent SSP. (a) Ambiguity surface for deep receiver localizing to a source location at 8.8 km, 75 m deep. Spatial sampling 171X150. All 2048 data are points used.(b) Ambiguity surface for shallow receiver localizing to a sourcelocation at 8.8 km, 75 m deep. Spatial sampling 171X150. All 2048 data points are used. No match.

(c)

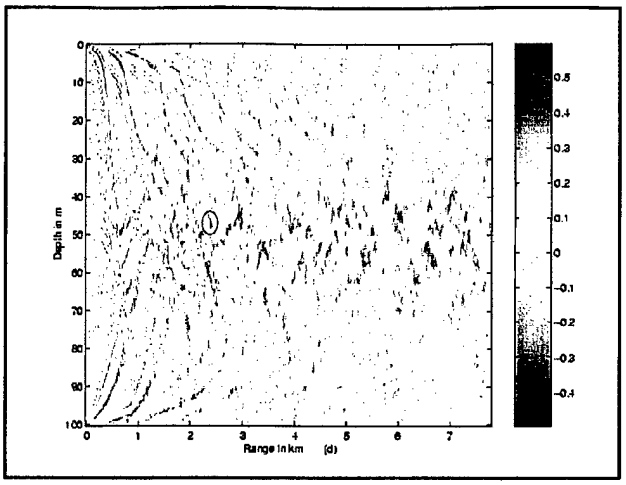

Figure IV.B.6 (continued): TACM for Case 6 with range dependent SSP. (c) Ambiguity surface for deep receiver localizing to a source location at 2.4 km, 47 m deep. Spatial sampling 171X150. All 2048 data points are used.

(d)

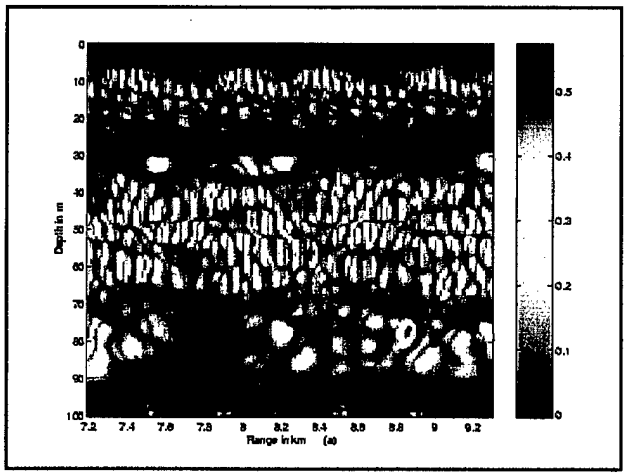

Figure IV.B.6 (continued): FACM for Case 6. (d) Ambiguity surface for deep receiver localizing to a source location at 8.8 km, 75 m deep. Spatial sampling 171X150. All data points are used.

(e)

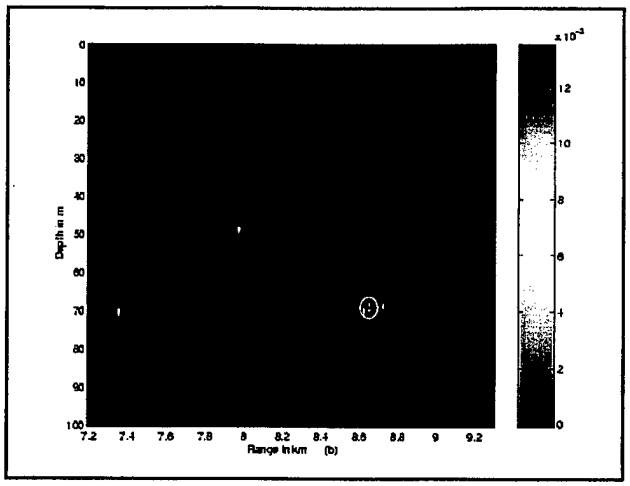

(f)

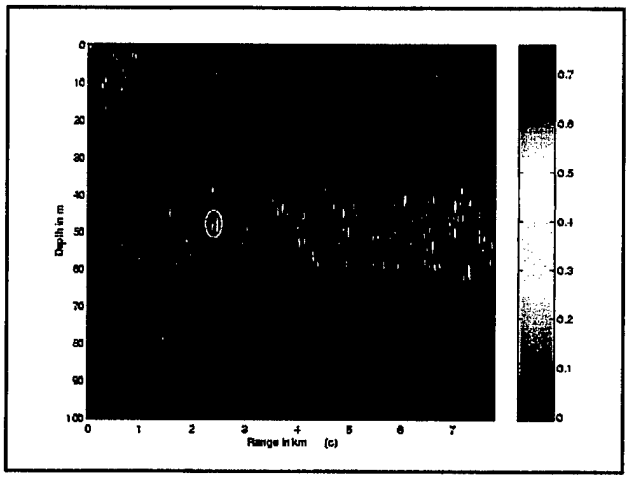

Figure IV.B.6 (continued): FACM for Case 6. (e) Same as (d) with shallow receiver. Values raised to the fifth power. (f) Ambiguity surface for deep receiver localizing to a source location at 2.4 km, 47 m deep. Spatial sampling 171X500. Every fourth data point is used. Values raised to the fifth power.

B.7. Case 7: Range-dependent SSP perturbed by internal wave soliton field from 2.5 to 8 km

The sound speed structure used to produce the synthetic measured signals for this case was extracted from the experimental data set between ranges 5 km and 15 km (refer to Fig. IV.B.5(a)). This produced an environment perturbed by the soliton packet from about 2.5 km to 8 km from the receiver arrays. Again, the environment was fixed relative to the receiver range, and only an average, range-independent SSP and bottom depth were used in the generation of the replica fields.

For source locations closer than the soliton field and above the SOFAR channel, the localizations were rather poor for both TACM and FACM as seen in Figs. IV.B.7(a) and (d). However, the footprint-size and peak-to-sidelobe levels were once again better for the FACM (4 m x 64 m, 1 dB) than for the TACM (3 m x 32 m, 0.4 dB). For the TACM method, the values on the ambiguity surface had to be raised to the fifth power in order to make the peak distinctively visible. This underscores the superiority of the FACM over the TACM in the presence of mismatch.

For the source locations beyond the range of the soliton field and within the SOFAR channel, a good localization could be made with both FACM and TACM as displayed in Figs. IV.B.7(c) and (f). In this unusual case, the TACM even provided slightly better results.

For the source locations within the soliton field, the closer source could be located, as seen in Figs. IV.B.7(b) and (e), whereas the source further away could not be localized by either algorithm. As in Case 5 and Case 6 the relative source and receiver locations were important for the goodness of the match.

Generally, it can be stated that the presence of such strongly range-dependent perturbations does affect the results significantly, and that the results get worse the larger the perturbations are.

(a)

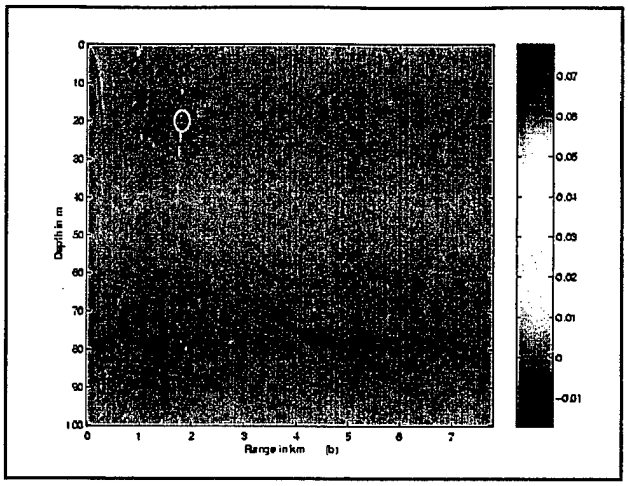

(b)

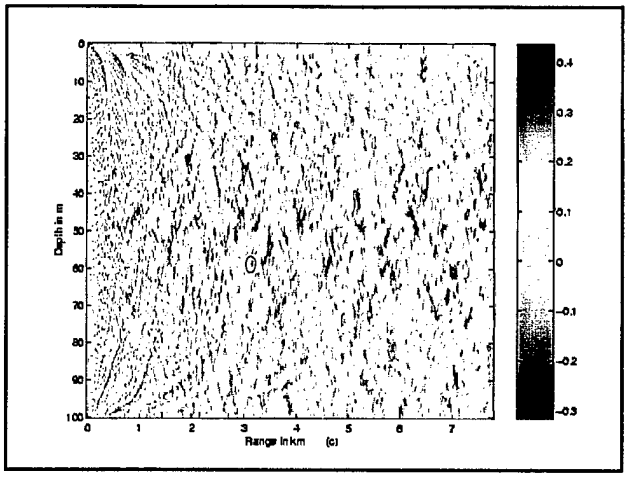

Figure IV.B.7: TACM for Case 7 with mismatch in sound speed profile (range dependence). (a) Ambiguity surface for shallow receiver localizing to a source location at 1.8 km, 20 m deep (before soliton field). Spatial sampling 171X500. All 2048 data points are used. Values raised to fifth power. (b) Ambiguity surface for deep receiver localizing to a source location at 3.2 km, 58 m deep (within soliton field). Spatial sampling 171X500. All 2048 data points used.

(c)

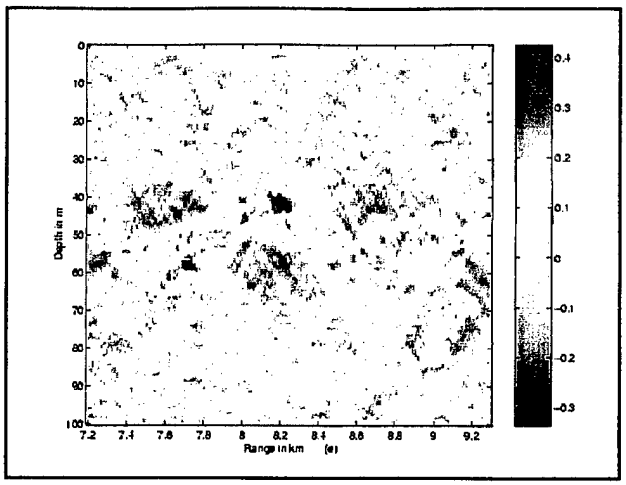

Figure IV.B.7 (continued): TACM for Case 7 with mismatch in sound speed profile (range dependence). (c) Ambiguity surface for deep receiver localizing to a source location at 8.1 km, 42 m deep (just behind soliton field). Spatial sampling 171X150. All 2048 data points used.

(d)

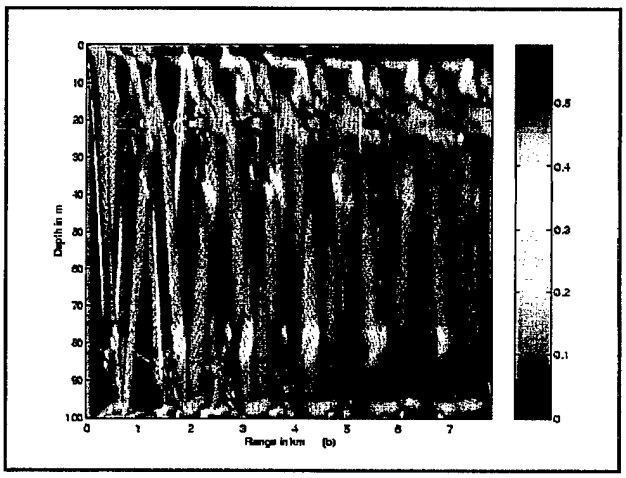

Figure IV.B.7 (continued): FACM for Case 7. (d) Ambiguity surface for shallow receiver localizing to a source location at 1.8 km, 20 m deep. Spatial sampling 171X150. All data points are used. Values raised to the fifth power.

(e)

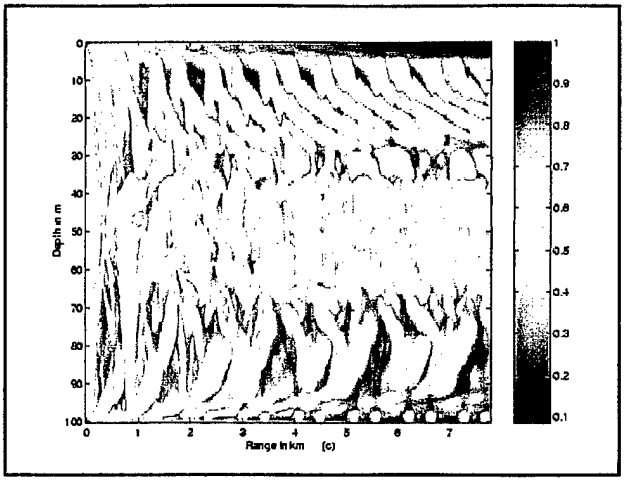

Figure IV.B.7 (continued): FACM for Case 7. (e) Ambiguity surface for deep receiver localizing to a source location at 3.2 km, 58 m deep. Spatial sampling 171X500. Every fourth data point is used.

(f)

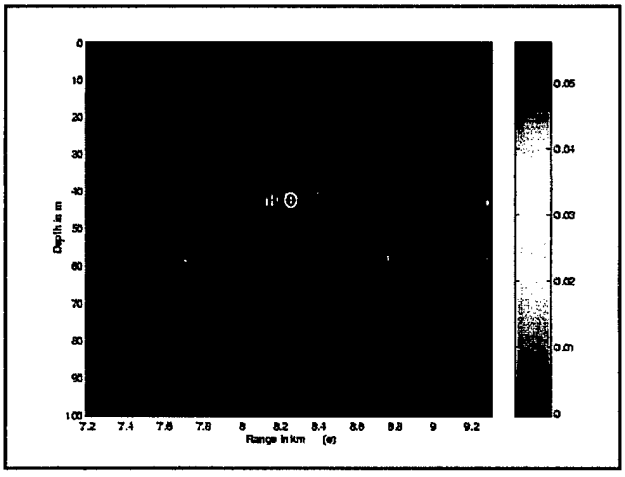

Figure IV.B.7 (continued): FACM for Case 7. (f) Ambiguity surface for deep receiver localizing to a source location at 8.1 km, 42 m deep. Spatial sampling 171X500. Every fourth data point is used. Values raised to the fifth power.

C. LOGARITHMIC FREQUENCY-DOMAIN AND TIME-DOMAIN AUTOCORRELATION MATCHING

In an attempt to enhance the significance of later, weaker arrivals, logarithmic versions of TACM and FACM were implemented (see Chapter III). However, it was found that such an approach degraded previous results where successful localizations had been made. Figure C.1 shows the results obtained for the easiest case (Case 1). It is obvious that for this case, a perfectly known and spatially well sampled environment, the footprint size and the peak-to-sidelobe levels are much worse using the logarithmic algorithms than the standard TACM and FACM. For this case, the peaks can be enhanced so that a distinct localization can be made. But in all other cases no match could be found with either logarithmic algorithm. Therefore, no further results from these logarithmic algorithms will be discussed.

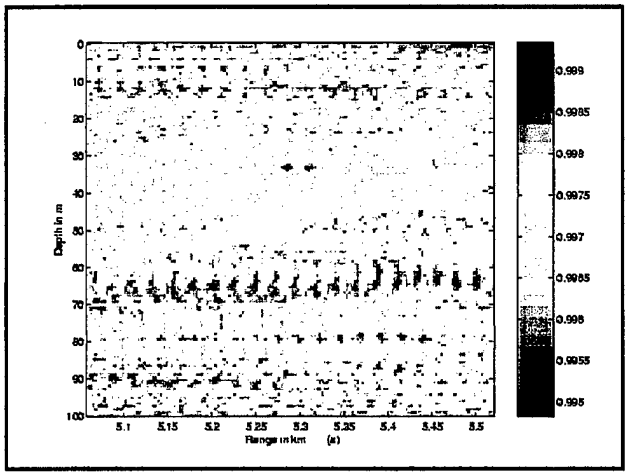

(a)

Figure IV.C.1: Logarithmic Autocorrelation Matching. (a) Frequency-Domain Autocorrelation Matching. Ambiguity surface for shallow receiver localizing to a source location at 5.3 km, 33 m deep. Spatial sampling 128X150. All data points are used.

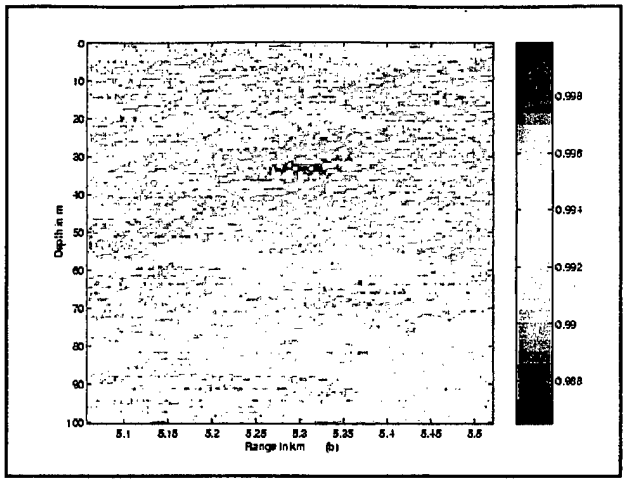

Figure IV.C.1 (continued): Logarithmic Autocorrelation Matching. (b) Same as (a) for Time-Domain Autocorrelation Matching.

D. Influence of noise on the performance of algorithms

So far, all of the synthetic data discussed in this chapter have been noise-free. This section investigates the effect of adding white noise to the synthetic data with regard to the consistency of the algorithms. In other words, how much noise can be added to the signal so that a localization is still possible in those cases where successful localizations occurred in the absence of noise? For this analysis, three different cases where localizations could originally be made for both TACM and FACM were investigated. The level of added white noise was varied such that the signal-to-noise ratio (SNR) was reduced from 20 dB down to - 20 dB. The SNR is defined as the average signal power divided by the average noise power (Oppenheim, 1983). Figure IV.D.1 shows the time-domain and frequency-domain signals with the added noise at the receiver locations for Case 1.

(a)

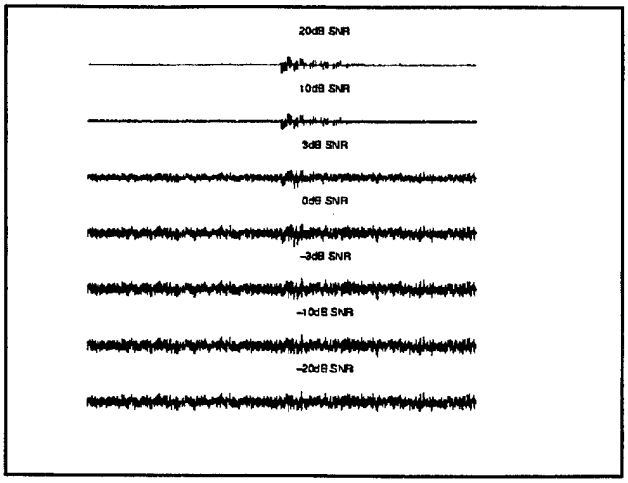

(b)

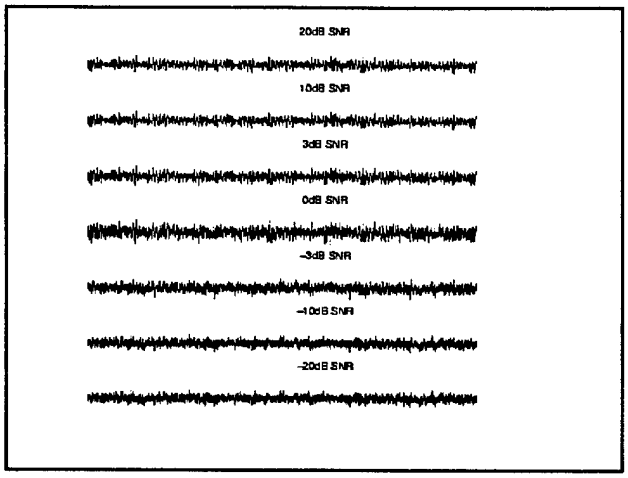

Figure IV.D.1: (a) Time-signal 0 to 1.38 sec. at receiver for source at 5.3 km 33 m deep for Case 1 (isospeed SSP) for different signal-to-noise ratios. (b) Frequency spectrum (500-2300 Hz) of time-signal.

For Case 1 where the environment is perfectly well known and the search grid spatially well sampled, the results show that for the FACM algorithm a good localization can still be made

for an SNR down to -3 dB. At an SNR of -10 dB, no localization can be made. For the TACM algorithm, good localizations can be made down to an SNR of 0 dB. From -3 dB down, the localization becomes very poor to impossible. This confirms once again that the FACM is more robust against uncertainties than the TACM as seen in Fig. IV.D.2.

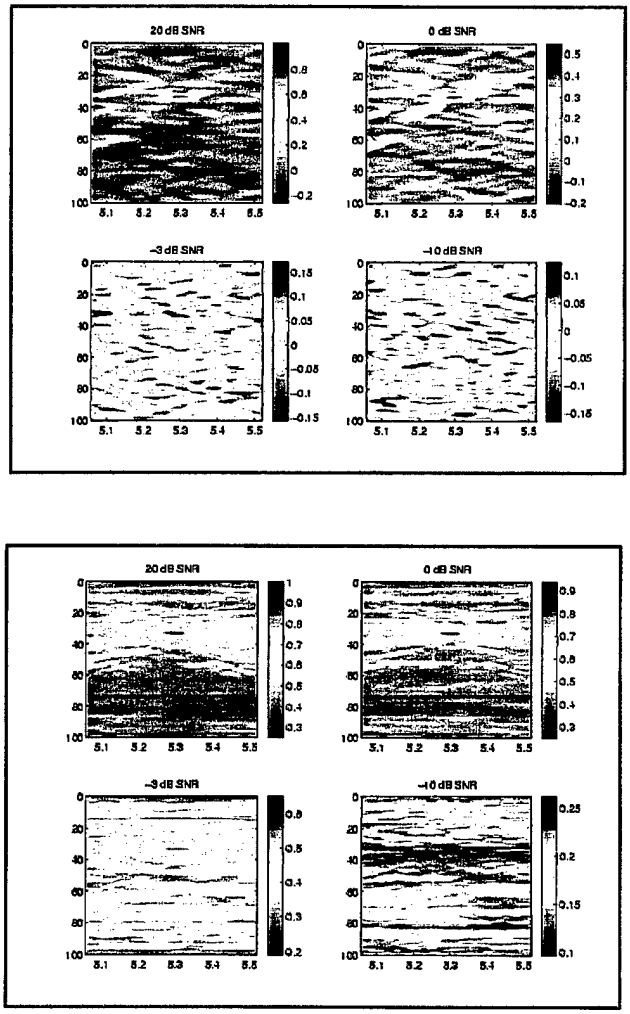

Figure IV.D.2: (a) TACM. Ambiguity surfaces for source at 5.3 km, 33 m deep for Case 1 (isospeed SSP) for different levels of SNR. (b) FACM. Ambiguity surfaces for source at 5.3 km, 33 m deep for Case 1 (isospeed SSP) for different levels of SNR.

For Case 2 with a nearly isospeed SSP and an uncertainty in the SSP, the results are basically the same as for Case 1. Again, the localization works well down to -3 dB SNR for the FACM, which performs better than the TACM, as displayed in Fig. IV.D.3. It can also be seen that the results in Case 2 are worse as compared to Case 1 for the same SNR's which is due to the fact that the search grid is spatially undersampled and a slight mismatch exists in the SSP.

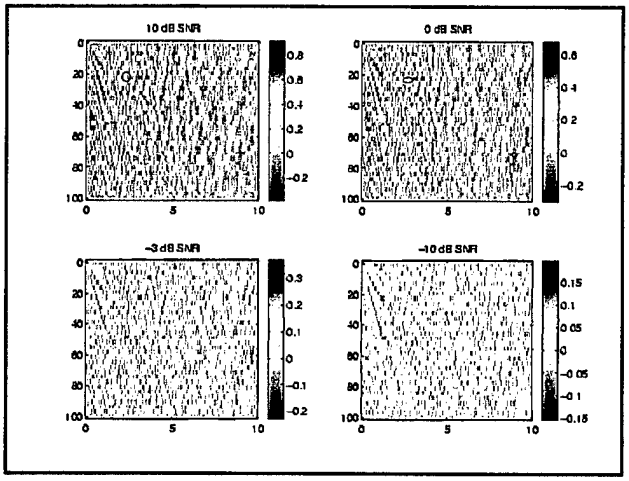

(a)

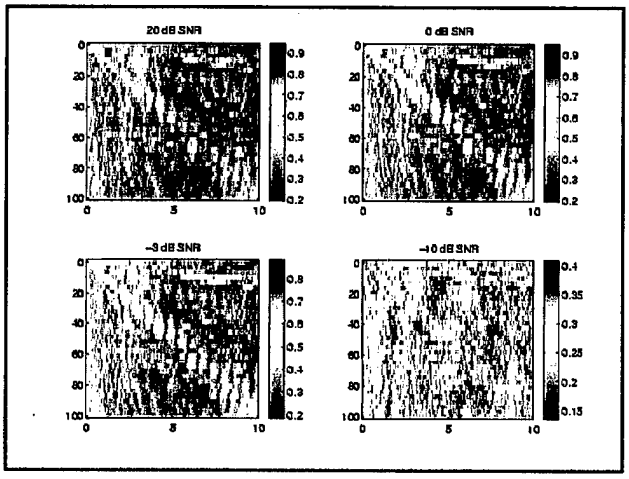

(b)

Figure IV.D.3: (a) TACM. Ambiguity surfaces for source at 3.1 km, 22 m deep for Case 2 (isospeed SSP, uncertainty in SSP) for different levels of SNR. (b) FACM. Ambiguity surfaces for source at 3.1 km, 22 m deep for Case 2 (isospeed SSP, uncertainty in SSP) for different levels of SNR.

The last case to which noise was added was one data set from Case 7 which contains a mismatch in bathymetry as well as a range-dependent mismatch in SSP due to the presence of a packet of solitons. The specific data set examined was one for which only a poor localization with low peak-to-sidelobe levels was possible for both TACM and FACM without noise. For the FACM a reasonable localization could still be made for -3dB SNR despite the significant environmental mismatches already present, as seen in Fig. IV.D.4. All of these results suggest that the influence of environmental mismatch has a more significant effect on the localization results than the presence of noise. It also suggests that, as long as the noise level is not higher than the signal level, the results will not be significantly affected by the presence of noise. This result is not entirely unexpected since the majority of the noise influence in the autocorrelation function occurs at zero lag which has been removed in both TACM and FACM algorithms. In the real world, a detected signal in noise will usually not have negative SNR. Otherwise, a detection would be rather improbable in the first place.

For the TACM, the results were similar to the FACM although continuing to show less robustness than the FACM, as displayed in Fig. IV.D.4. The TACM fails to make localizations at an SNR of -3 dB whereas the FACM still worked well. At an SNR of 0 dB, the TACM localization is very poor.

(a)

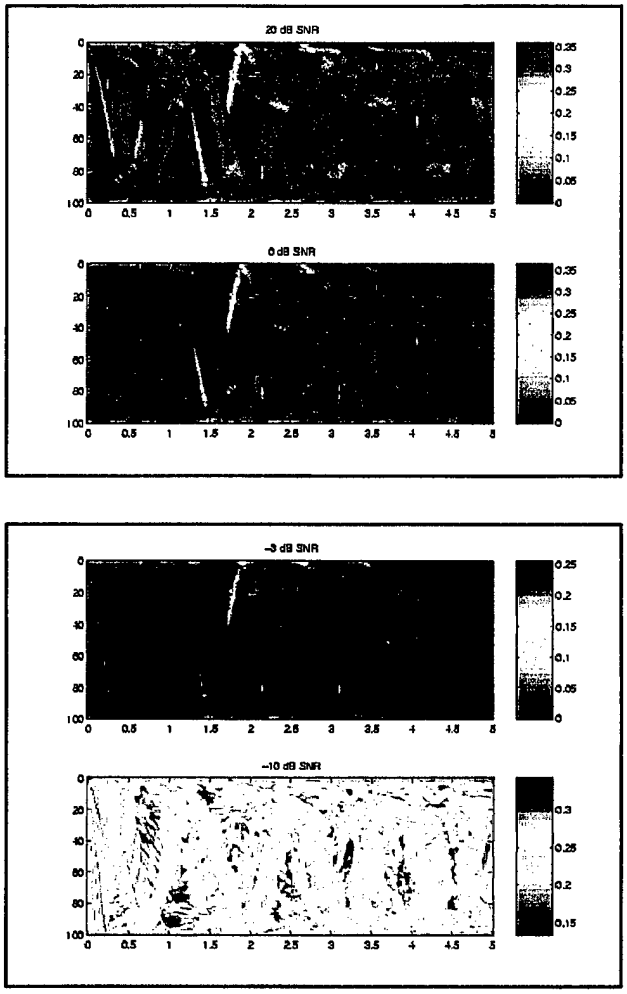

Figure IV.D.4: (a) FACM. Ambiguity surfaces for source at 1.8 km, 20 m deep for Case 7 with mismatch in SSP and bathymetry for different levels of SNR.

(b)

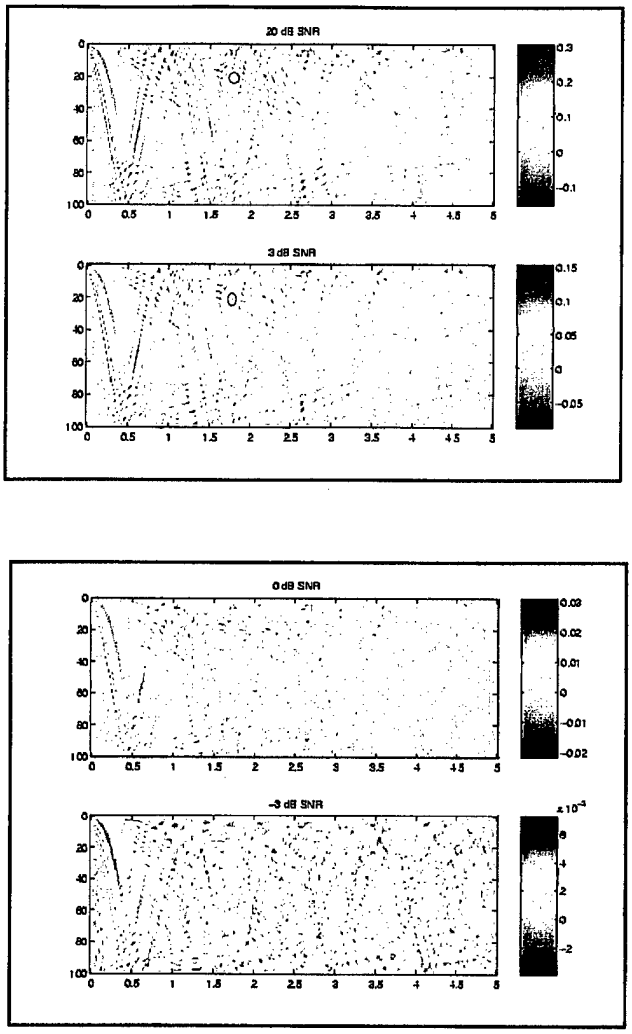

Figure IV.D.4 (continued): (b) TACM. Ambiguity surfaces for source at 1.8 km, 20 m deep for Case 7 (Mismatch in SSP and bathymetry) for different levels of SNR.

E. Effect of bandwidth in the presence of noise

In this section, the effect of a reduction in the bandwidth on the results as obtained in Section IV.D is analyzed. The scenario of Case 2 was chosen as a representative environment. For both algorithms, TACM and FACM, a good localization was still possible for the spatially undersampled case with an SNR of -3 dB (see previous section). Thus the noise-level used in this experiment was fixed to -3 dB SNR, and the bandwidth was varied for both algorithms to find the limits of a possible localization.

Figures IV.E.1(a-h) show the results for the TACM. The TACM worked best, as shown previously, for lower frequency bands. A localization was still possible for a bandwidth of only 225 Hz, from 500 Hz to 725 Hz, which is equal to just one eighth of the full bandwidth with 256 data points as seen in Figs. IV.E.1(a) and (b). Considering only the lowest sixteenth of the bandwidth, 500 to 612.5 Hz, led to no localization. This may be due to fewer arrivals being adequately resolved at smaller bandwidths which causes the autocorrelation and its match to drop off rapidly away from the source location.

When sampling the full bandwidth at only every fourth and every eighth point, localizations could still be made despite being rather poor. For sampling only every sixteenth data point of the full bandwidth, there was still a relative peak at the correct location but the absolute maximum was found elsewhere as seen in Fig. IV.E.1(c). The undersampling introduces aliasing effects and severe wrap-around in the time-domain of the autocorrelation functions so that a localization with these degraded functions becomes impossible. Looking at only the lower half and the upper half of the bandwidth and sampling only every fourth data point still provided a correct localization, although footprints and peak-to-sidelobe levels were very poor, as seen in Figs. IV.E.1(d-h).

Summarizing the results for the TACM, it can be stated that it works best in the low frequency region, and that a bandwidth of only a few hundred Hertz (in this case one eighth of the total bandwidth) is sufficient to provide reasonable localization matches even for a SNR of -3 dB. It should not be forgotten, however, that the environmental mismatch in this case was only of little significance.

(a)

(b)

(c)

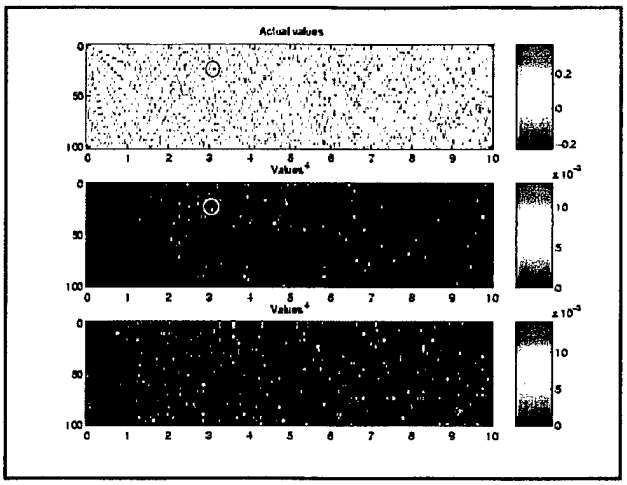

Figure IV.E.1: TACM. Ambiguity surfaces for source at 3.1 km, 22m deep for Case 2 with SNR of - 3dB. (a) first quarter of full bandwidth (500-950Hz), (b) first eighth of full bandwidth (500-725Hz), (c) first sixteenth of full bandwidth (500-612.5 Hz), no match.

(d)

(e)

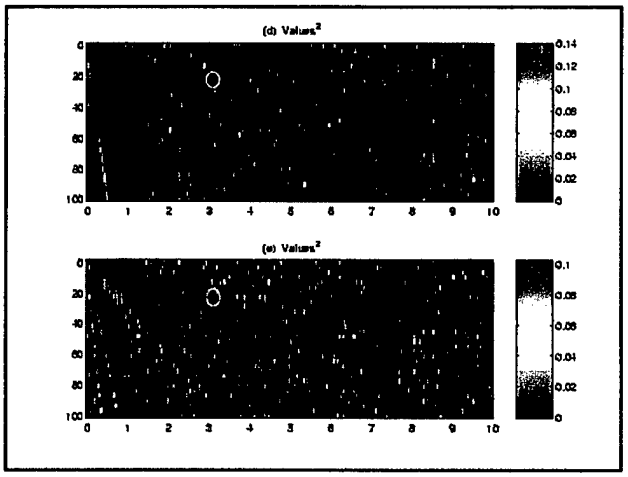

Figure IV.E.1 (continued): TACM. Ambiguity surfaces for source at 3.1 km, 22 m deep for Case 2 with SNR of - 3dB. (d) lower half of full bandwidth, every fourth data point is used, (e) upper half of full bandwidth, every fourth data point is used.

(f)

(g)

(h)

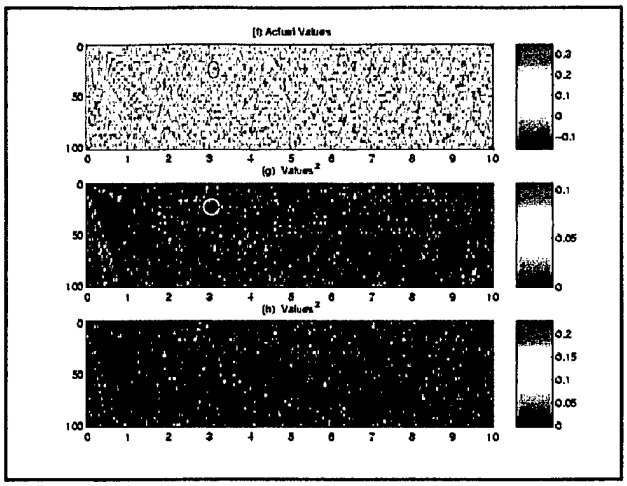

Figure IV.E.1 (continued): TACM. Ambiguity surfaces for source at 3.1 km, 22 m deep for Case 2 with SNR of - 3dB. (f) full bandwidth, every fourth data point is used, (g) full bandwidth, every eighth data point is used, (h) full bandwidth, every sixteenth data point is used.

For the FACM, the results show that the best localizations can be made when the full bandwidth of the signal is exploited, as suggested previously. Again, the Case 2 scenario was chosen as a representative environment. When sampling down to every eighth point, good matches are still obtained as seen in Figs. IV.E.2(a-c).

To examine the performance of the FACM algorithm for smaller bandwidths, calculations were made for half of the original bandwidth including the lower half (500 Hz-1400 Hz), the middle half (950 Hz-1850 Hz), and the upper half (1400 Hz-2300 Hz). The results, as displayed in Figs. E2 (d)-(f), illustrate that the FACM algorithm works much better for the higher frequencies than for the lower frequencies. This may be due to the increased complexity at higher frequencies leading to more unique structures in the autocorrelation function. The best results, however, are reached when sampling the middle of the bandwidth. Finally, when only one quarter of the bandwidth is used, the results become much worse as seen in Figs. IV.E.2(g-i). For smaller bandwidths, no localizations could be made.

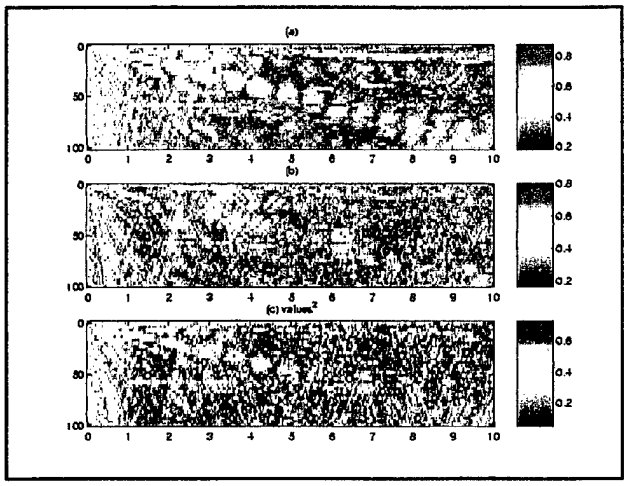

(a)

(b)

(c)

Figure IV.E.2: FACM. Ambiguity surfaces for source at 3.1 km, 22 m deep for Case 2 with SNR of - 3dB. (a) full bandwidth, every fourth data point is used, (b) full bandwidth, every eighth data point is used, (c) full bandwidth, every sixteenth data point is used.

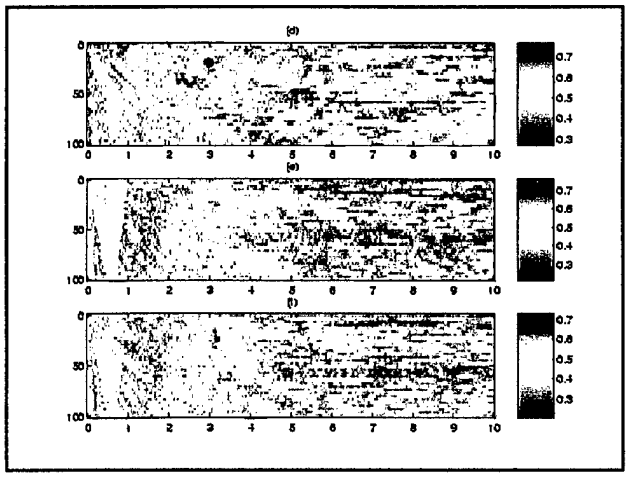

(d)

(e)

(f)

Figure IV.E.2 (continued): FACM. Ambiguity surfaces for source at 3.1 km, 22 m deep for Case 2 for SNR of - 3dB. (d) lower half bandwidth, every second data point is used, (e) middle half bandwidth, every second data point is used, (f) upper half bandwidth, every second data point is used.

(g)

(h)

(i)

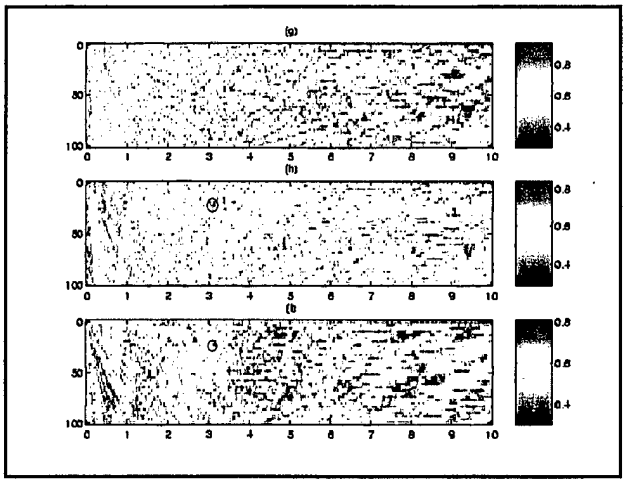

Figure IV.E.2 (continued): FACM. Ambiguity surfaces for source at 3.1 km, 22 m deep for Case 2 with SNR of - 3dB. (g) upper quarter bandwidth, every second data point is used, no match. (h) same as (g) with all data points used, (i) middle quarter bandwidth, all data points are used.

F. Summary of synthetic data results

The FACM algorithm provided a larger footprint size and higher peak-to-sidelobe levels in nearly all synthetic cases as compared to the TACM. The TACM is generally more useful for smaller bandwidths at low frequencies, whereas the FACM is better suited for larger bandwidths and higher frequencies. The FACM proved to be more robust against environmental mismatches, added white noise, and spatial undersampling than the TACM. The influence of environmental mismatch has a much more significant effect on the localization results than the presence of noise for both algorithms. This is to be expected, since for white noise the majority of the influence on the autocorrelation function occurs at zero lag which has been removed in both TACM and FACM algorithms. Good localizations even in the presence of severe environmental mismatch could still be made with both algorithms for SNR's down to at least -3 dB.

For good localization results the knowledge of the SSP is more crucial than the estimate

of any other environmental parameter. Furthermore, the best localization results are obtained in isospeed environments followed by environments with a SOFAR channel. In this case the relative location of source and receiver are critical for good results. Good localizations could be made with either both source and receiver in the channel or both source and receiver outside the channel. Environments characterized by positive, upward refracting sound speed gradients are generally more favorable than environments with negative, downward refracting sound speed gradients which represent the most difficult localization environment.

The FACM provided correct localizations for almost all cases and for many scenarios in which the TACM was unsuccessful. Improved spatial sampling or techniques such as zero-padding the signal to twice its length which, of course, increase the necessary computational time, improved the results for the FACM in the more difficult scenarios.

V. REAL DATA RESULTS

In this section, the results of the analysis of some real broadband explosive SUS data taken from the Mid-Atlantic Bight Field Study (Pickart, et al.,1996) are presented. The Mid-Atlantic Bight Field Study, also known as Primer experiment, was a collaborative shallow water acoustics experiment between the Woods Hole Oceanographic Institute, the University of Rhode Island, and the Naval Postgraduate School. The purpose was to study the influence of a highly variable, strongly 3-D, shallow water environment on acoustic propagation. Among the assets used were 61 P-3 SUS deployments, and two 16-element vertical receiver arrays. For this work, recorded data of a SUS detonation about 6.5 km away from the Vertical Line Array (VLA) in the NW-corner of the study area were analyzed.

Unfortunately, no sound speed data were available directly at the receiver. In order to define a typical sound speed profile near the VLA, several measured sound speed profiles closest to the receiver were averaged. The SSP used for the generation of the replica signals is displayed in Fig. V.1.

Bottom depth values from the VLA towards the direction of the SUS drop, approximately along a 90 m isobath, were extracted from a bathymetry data base of the region. Bottom properties such as sound speed, sound speed gradient, density, attenuation and shear were not exactly known, so reasonable parameters for typical continental shelf sediments were used. Specifically, values chosen were compressional sound speed c_b =1600m/s, no compressional sound speed gradient, a density and attenuation ϱ_b= 1.5 g/cm^3 and α_b= 0.10 dB/km/Hz. Shear was neglected and the water was assumed to have a density of 1.0 g/cm^3.

During the course of the SUS deployment, only the upper 8 hydrophones of the NW VLA functioned properly. The depths of these phones spanned from 30.5 m to 55 m with inter-element spacing of 3.5 m. The sampling frequency of the SUS data was recorded at 3906.25 Hz. The SUS charges were 1.2 lb of TNT explosive designed to detonate at a depth of 18.3 m.

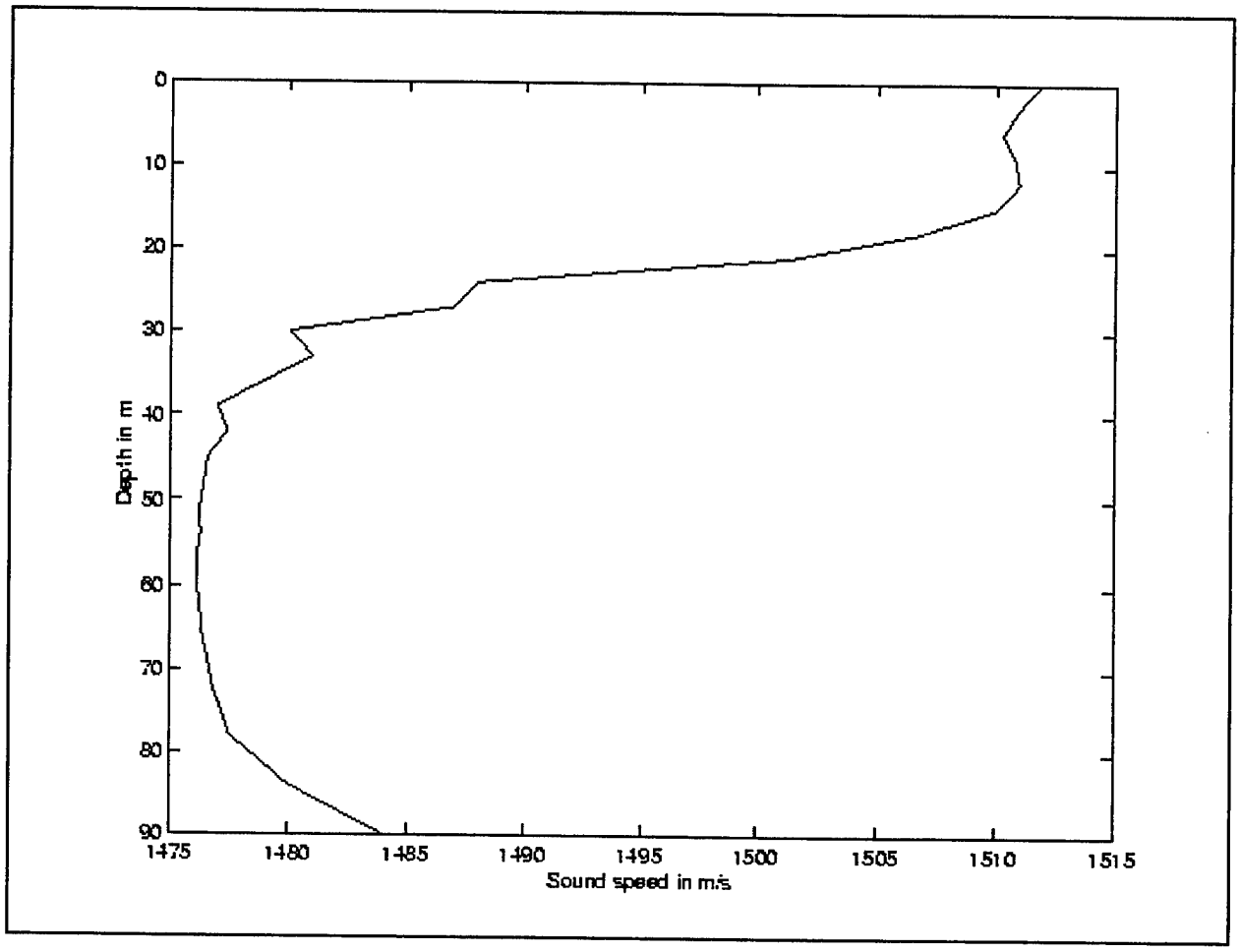

Figure V.1: Averaged continental shelf water sound speed profile of Mid-Atlantic Bight Field Study.

As can be seen from the sound speed data displayed in Fig. V.1, there was a sound channel axis present in the region that spanned from about 28 m down to the bottom depth of 90 m. The top receiver of the array was therefore in the channel while the SUS source detonation was above the channel. Based on the results from the synthetic data sets, this would be considered a very unfavourable situation, especially when much uncertainty might exist in the

SSP and the bottom parameters.

Figure V.2 shows the time sequence of the recorded signal on the top hydrophone of the NW VLA shortly after the SUS explosion.

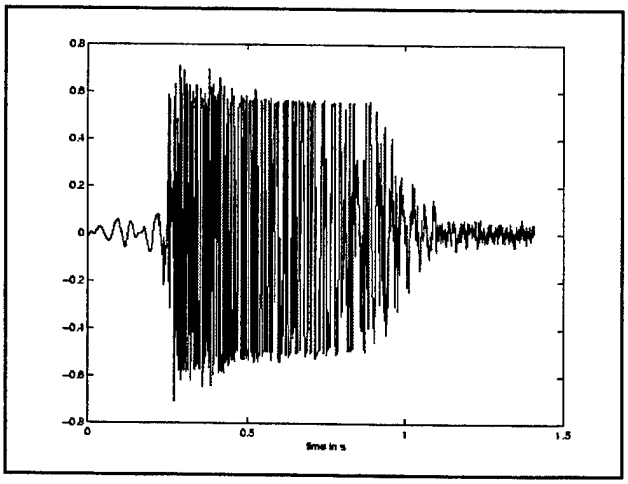

Figure V.2: Real valued time-sequence of recorded SUS data

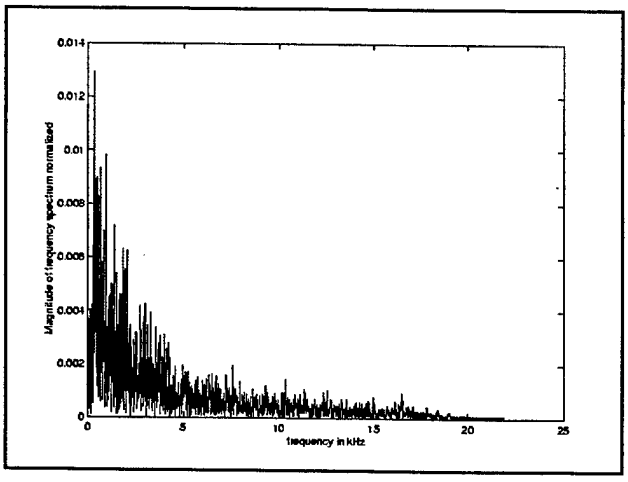

Figure V.3: Frequency spectrum of recorded SUS data

The recorded signal was sampled at 3906.25 Hz over a length of 8.3886 seconds. Figure V.3 shows the frequency spectrum of the recorded signal which illustrates that the low frequencies are dominant and that major contributions of the energy of the signal lie within the frequency band below 500 Hz. To be able to use the matching algorithms as before, the recorded signal was sampled and multiplied by a shifted Hanning window in order to reduce the signal to a length of 2048 spectral points over a bandwidth of 500 Hz to 2300 Hz.

When the search grid was drastically undersampled spatially the results were unsatisfactory. No localization could be made. For a spatially well sampled acoustic field and the shallowest receiver (30.5 m), however, the FACM algorithm made a good localization whereas the TACM located the source a little too shallow and a bit too far out as displayed in Figs. V.4(a) and (b). Attempts to improve the localization results by decreasing the minimum frequency down to 200 Hz rather than 500 Hz were unsuccessful. The spatial sampling of the environment proved to be the determining factor for a good match. Again, the FACM produced better results than the TACM. Attempts to localize the source with the deep receiver did not provide the desired results. However, for the FACM there still appears a relative peak at the correct location, and for the TACM the peak value appears at the correct range but on the surface instead of 18.3 m deep, as seen in Figs. V.4(c) and (d). The spatial sampling was the same as for the shallow receiver.

(a)

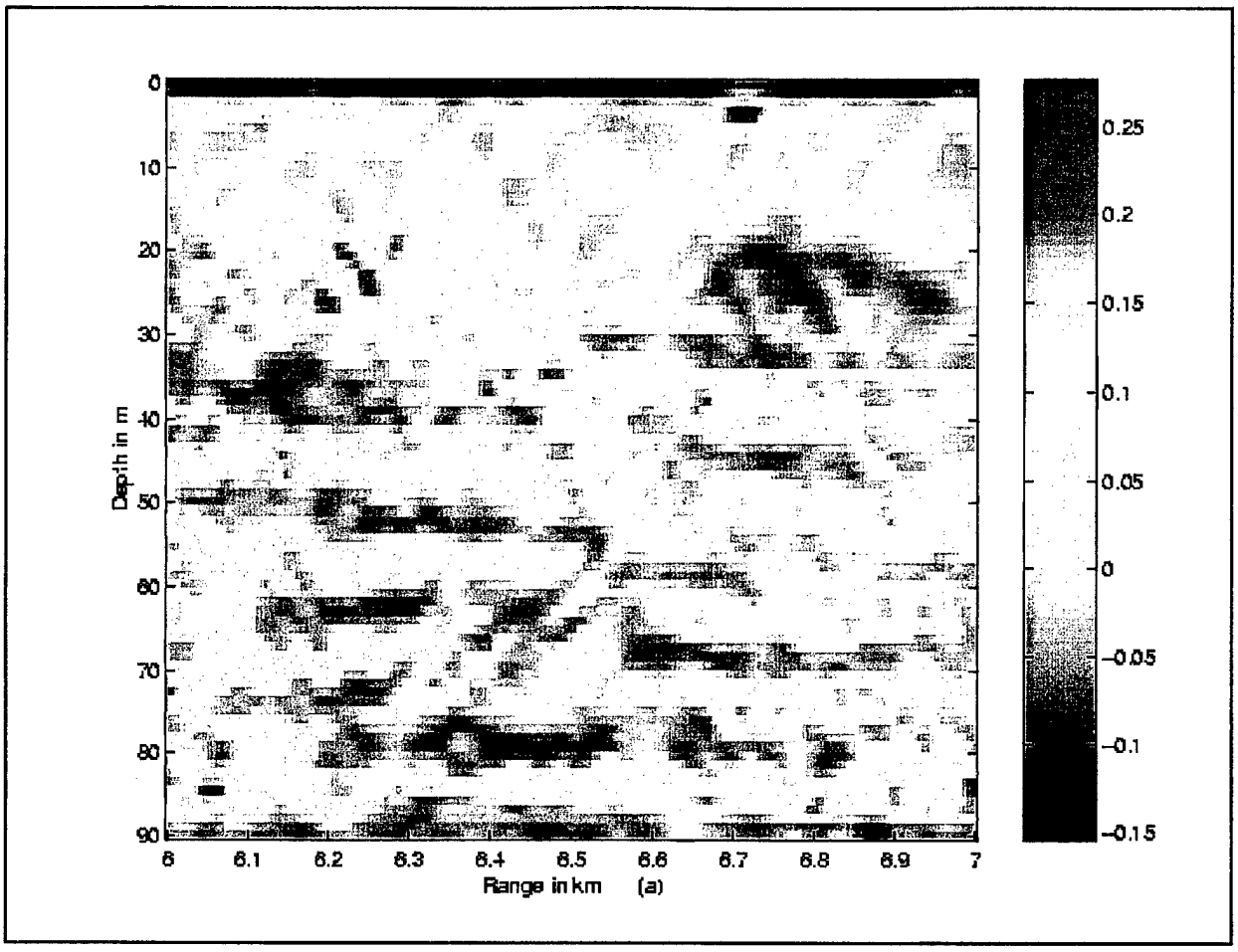

Figure V.4:(a) TACM. Ambiguity surface for Primer experiment, source location approximately at 6.48 km, 18.3 m deep, receiver at 30.5 m, spatial sampling 86X200.

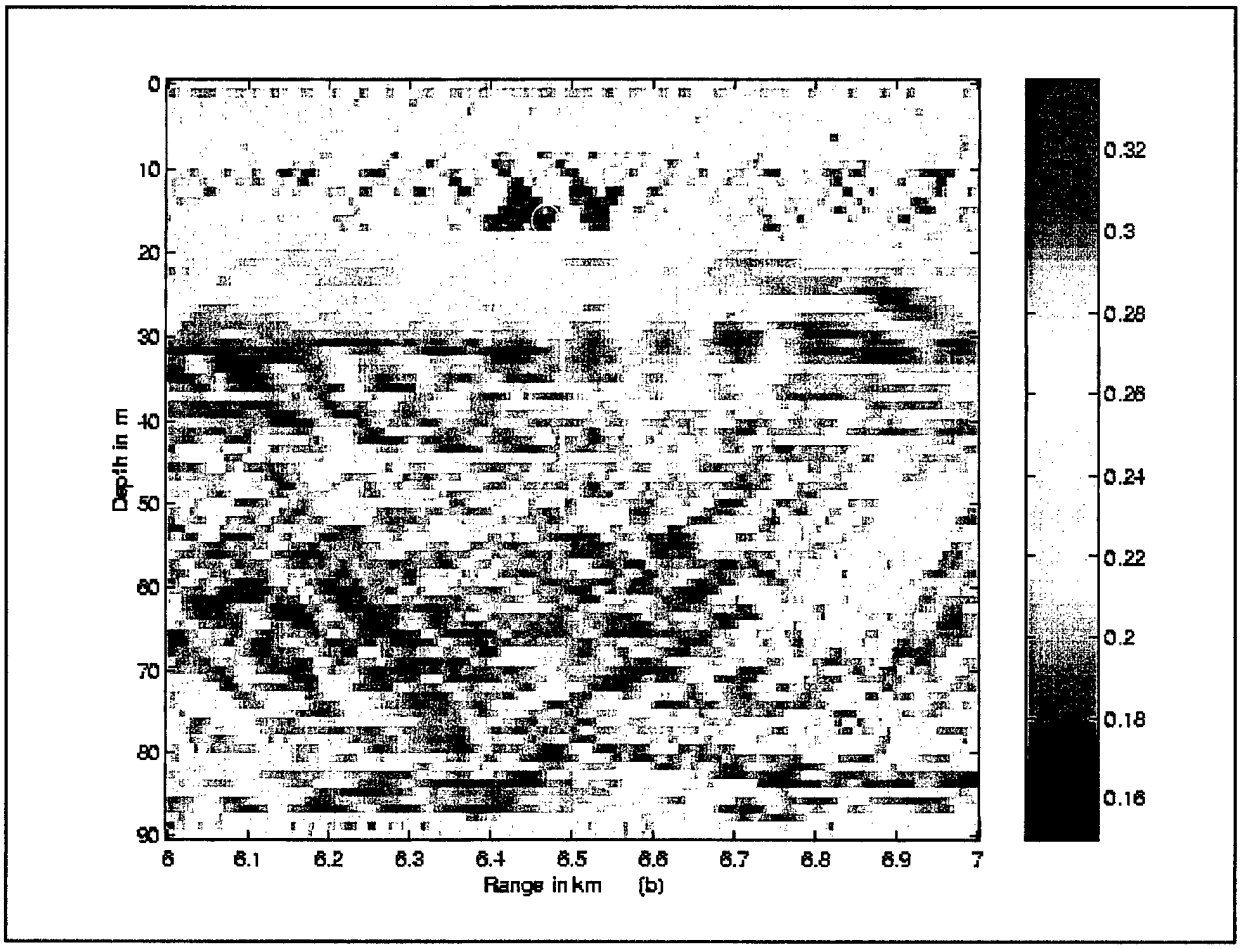

Figure V.4 (continued):(b) FACM. Ambiguity surface for Primer experiment, source location approximately at 6.48 km, 18.3 m deep, receiver at 30.5 m, spatial sampling 86X200.

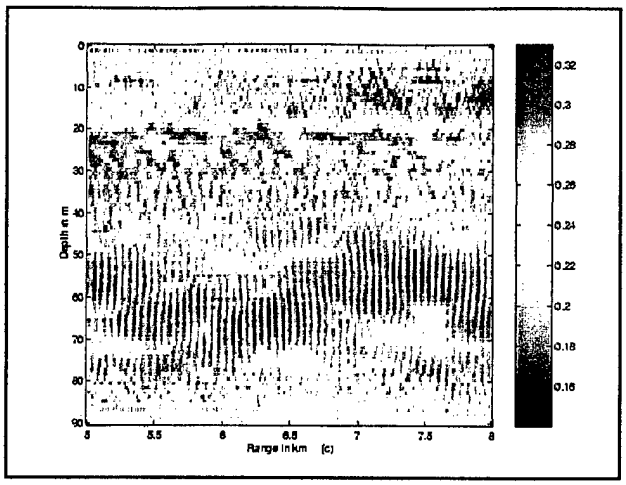

(c)

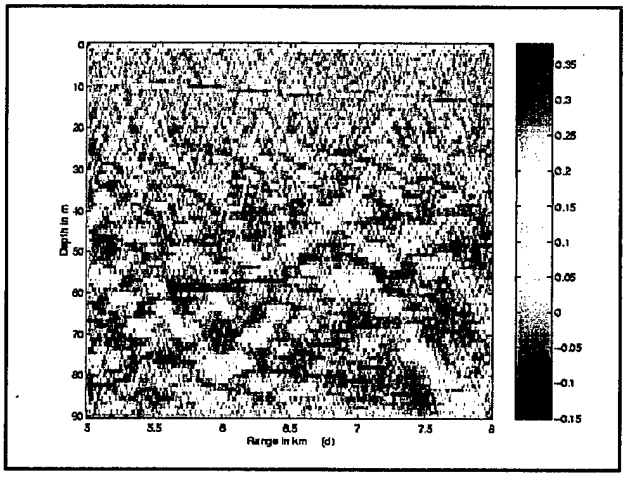

(d)

Figure V.4 (continued):(c) FACM. Ambiguity surface for Primer experiment, source location approximately at 6.48 km, 18.3 m deep, receiver at 55 m, spatial sampling 86X300.
(d) TACM. Ambiguity surface for Primer experiment, source location approximately at 6.48 km, 18.3 m deep, receiver at 55 m, spatial sampling 86X300.

Finally, an attempt was made to estimate the original signal from the replica signal where the localization was made as a consistency check on the quality of the localization. The measured signal can be represented by the product A(f)g(f) where A(f) is the source spectrum and g(f) is the ocean transfer function, or Green's function. In the previous analysis, the replicas have been defined by predictions of the ocean transfer function modulated by a simple Hanning window over the bandwidth of interest, i.e. H(f)g'(f). In the ideal case, the predictions are exact, g'(f) = g(f), and a localization at the correct location would provide the true ocean transfer function between source and receiver. This information could then be inverted to yield a prediction of the source spectrum, A(f). The receiver filter characteristics were assumed to be flat (no filtering) over the bandwidth considered.

In the case of the experiment considered here, the match, of course, was not perfect. However, the frequency spectrum of the reconstructed signal, using the method outlined above, is quite similar to what would be expected of a SUS source. Comparing the reconstructed spectrum to the spectrum of a similar 1 lb depth charge (Urick, 1975), as displayed in Figs. V.5(a) and (b), shows that the slopes of energy decay versus frequency match relatively well. Both drop by approximately 11 dB over one decade in bandwidth.

The overall results of this analysis with real data are promising, especially given the huge uncertainty in the environment, the unfavourable relative position of source and receiver, and the rather unfavourable frequency spectrum of the source with the power concentrated in the lower frequency band.

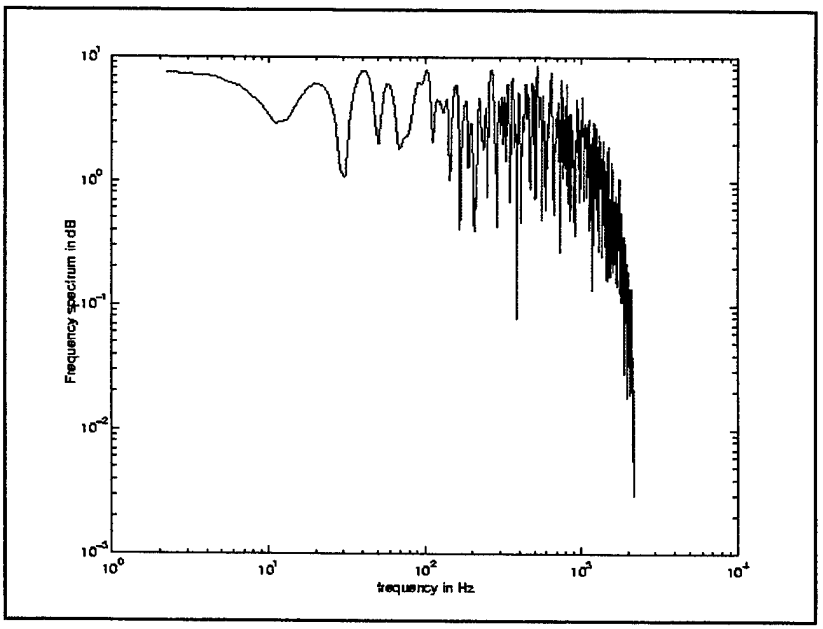

(a)

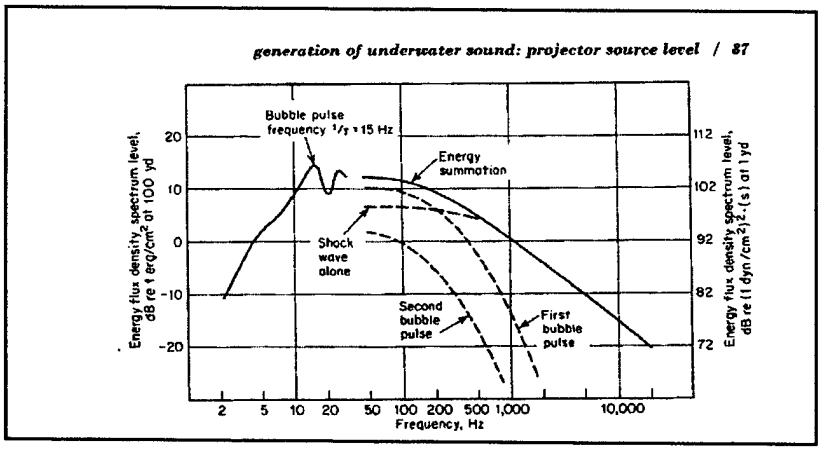

(b)

Figure V.5: (a) Frequency spectrum of the reconstructed original signal. (b) Spectrum of 1 lb depth charge taken from Urick (Principles of Underwater Sound, 1975)

VI. CONCLUSIONS

The synthetic data illustrate that the TACM is generally more useful for smaller bandwidths at low frequencies, which has been observed in previous work (de Kooter, 1997), whereas the FACM is better suited for larger bandwidths and higher frequencies. The footprint size for the FACM is generally larger than for the TACM, and the peak-to-sidelobe levels are mostly better for the FACM than for the TACM.

Better localization results were obtained when the environmental parameters were well known. However, with a large enough bandwidth the FACM seems fairly robust against environmental mismatch. Generally an uncertainty in the SSP seems to affect the results more than a mismatch in the bathymetry.

The relative position of source and receiver with respect to the SSP and bathymetry can affect the results significantly. Specifically, if there is a strong gradient or a sound channel, a rather advantageous relative positioning of source and receiver can improve the results vastly.

Another basic observation made is that better spatial sampling of the acoustic field leads to improved results for both FACM and TACM. Better spatial sampling, however, increases the computational effort and therefore the time needed to obtain the results. An ambiguity surface for a spatial resolution of 3.2 m in depth and 332 m in range with an environment of size 100 m x 10 km as used for most synthetic cases, could be created within less than 4 minutes with the available machine which is an operationally acceptable period of time. Certainly, with faster processors and more memory, this time can still be reduced. Also, the Matlab code used could at least partially be modified into C or C ++ which would probably further reduce the computation time. One could also split the environment into several spatial segments and run several routines at the same time, and thereby reduce the computional time needed to obtain a result and increase the probability of a good localization by using a better spatial sampling. A parallel run for both algorithms might be another way of improving results and computational time needed.

The preliminary localization results for the Mid-Atlantic Bight Field Study are quite encouraging. One might next want to look at some real data with lower SNR's than for the SUS, which was about 8 dB in the case considered here, and evaluate the robustness of the algorithms

then. The results in Section IV.D show, at least for synthetic data, that even at very low SNR the characteristics of a signal present in noise can still be exploited for a good localization. Noise seems to be less critical for a good localization than the amount of environmental mismatch, one of the primary advantages of using autocorrelation functions. Therefore, the algorithms can be expected to still work well for data with a fairly low SNR.

Another way of improving results proved to be the zero-padding of signals, especially for scenarios with fairly high environmental mismatch. This provides extra looks between actual data points and therefore provides some kind of artificially increased spatial sampling.

Throughout this work second order moments (Chapter III) were matched which is basically equivalent to the matching of instantaneous power (Hager, 1997). It was also attempted to match third order moments of the same quantities. The matched quantities, however, did not represent physically meaningful parameters and the third-order moment method was not successful. The same is true for the matching of just the complex pressure field data. Attempts at such a fully coherent matching, which represents a physically meaningful quantity, failed to produce good results as soon as environmental mismatch was introduced. Figure VI.1 shows the poor results for Case 2, the isospeed scenario with slight uncertainty in the SSP. Another difficulty that occurs when using either first or third order moments is the fact that the obtained values for the ambiguity surface are not real but complex quantities, so that one has to compare either the absolute values or the phase or just real or imaginary parts for the ambiguity surface. Neither the matching of absolute values nor the comparison of the real parts led to successful results.

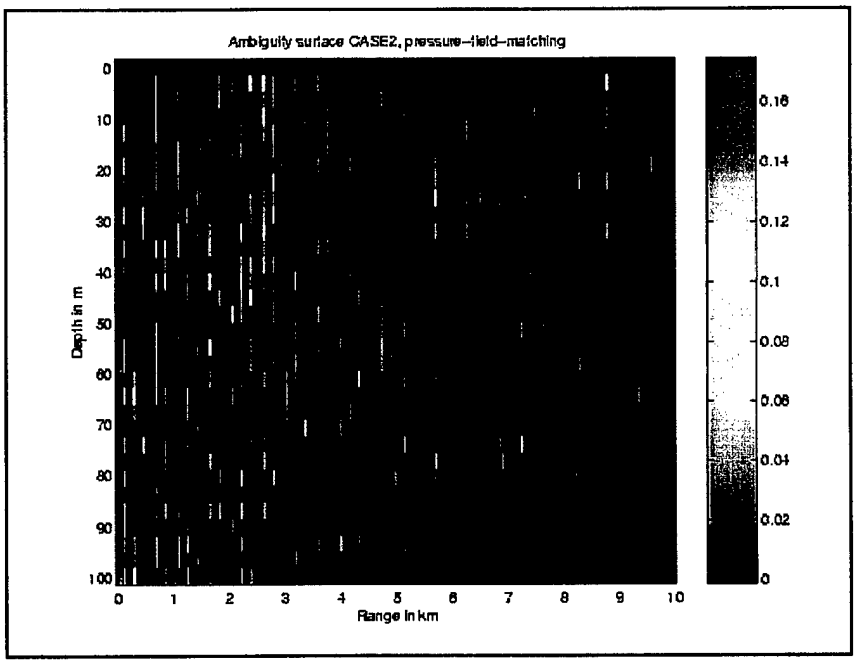

Figure VI.1: Case 2, Ambiguity surface for matched pressure field data, source at 3.1 km, 22 m deep, shallow receiver, spatial sampling 32X300. No match.

A last point to make is that neither of the logarithmic matching methods worked well. Instead of enhancing later, weaker arrivals these algorithms compressed all data on the ambiguity surface to values between 0.9990 and 0.9999, and the footprint sizes and peak-to-sidelobe levels were fairly poor. As soon as environmental mismatch was introduced these methods failed completely. This might be due to the fact that the weaker arrivals are probably more sensitive to mismatches. It therefore seems that this matching method will not lead to improved results in possible future work considering environments similar to those considered in this work.

LIST OF REFERENCES

Apel, J.R., Badiey, M., Chiu, C.-S., Finette, S., Headrick R., Kemp, J., Lynch, J.F., "An Overview of the 1995 SWARM Shallow-Water Internal Wave Acoustic Scattering Experiment," *IEEE Journal of Oceanic Engineering*, July 1997.

Bendat, J.S. and Piersol, A.G., *Random Data: Analysis and Measurement Procedures,* Wiley-Interscience, New York, 1971.

Benson, J.L.,"Time-Domain Localization of Transient Source in Shallow Water," Master's Thesis, Naval Postgraduate School, June 1995.

Chiu, C.-S., Ng, S.-L. and Denner, W.W., "Estimating the properties of the sound field in a shelf region near the shelfbreak," *Proceedings of the Sixth Western Pacific Regional Acoustics Conference*, Hong Kong, 1997.

Clay, C.S., "Optimum time domain signal transmission and source localization in a waveguide," *J. Acoust. Soc. Am.,* v. 81(3), 660-664, March 1987.

Hager, C.A., "Modeling the performance of the PT.SUR Hydrophone Array in Localizing Blue Whales," Master's Thesis, Naval Postgraduate School, September 1997.

Jensen, F.B., Kuperman, W.A.,Porter M.B. and Schmidt H., *Computational Ocean Acoustics,* American Institute of Physics Press, Woodbury, NY, 1994.

de Kooter, P.M., "Variations on Autocorrelation Matching and the SIFT Localization Algorithm," Master's Thesis, Naval Postgraduate School, March 1997.

Makris, N.C., "The effect of saturated transmission scintillation on ocean acoustic intensity measurements," *Journal of Acoustic Society of America*, August 1996.

Mathworks, Inc., " Matlab 5.0, User's Guide," Mathworks Inc, 1996.

Miller, J.H., Benson, J.L., Chiu, C-S., and Smith, K.B., *Transient Localization Project at the NPS,* Technical Report, Naval Postgraduate School, April 1996.

Oppenheim, A.V., Willsky, A.S., and Young, I.T., *Signals and Systems,* Prentice Hall, Englewood Cliffs, NJ, 1983.

Pickart, R.S., Gawarkiewicz, G.G., Lynch, J.F., Chiu, C.-S., Smith, K.B., and Miller, J.H., "Endeavor 286 Cruise Summary: PRIMER III," Naval Postgraduate School, August 1996.

Pierce, D.D., *Range-Dependent Passive Source Localization using data from the Barents Sea Tomography experiment,* Ph.D. Dissertation, Naval Postgraduate School, June 1996.

Press, W.H., Flannery, B.P., Teukolsky, S.A., and Vetterling, W.T., *Numerical Recipes,* Cambridge University Press, New York, NY, 1988.

Proakis, J.G., and Manolakis, D.G., *Digital Signal Processing,* Prentice Hall, Upper Saddle River, NJ, 1996.

Smith, K.B., Personal communication, Naval Postgraduate School, April 1996. The Monterey-Miami Parabolic Equation (MMPE) model is an upgraded version of the University of Miami Parabolic Equation (UMPE) model (Smith and Tappert, 1993).

Smith, K.B., and Tappert, F.D., *UMPE: The University of Miami Parabolic Equation Model, version 1.1*, MPL Technical Memorandum 432, May 1993 (revised edition September 1994), Marine Physical Laboratory, Scripps Institution of Oceanography, University of San Diego.

Tappert, F.D., "Parabolic equation method," in Lecture Notes in Physics, Vol.70, Wave Propagation and Underwater Acoustics, pp. 224-287, edited by J.B. Keller and J.S. Papadakis, Springer Verlag, New York, NY, 1977.

Thomson, D.J., and Chapman, N.R., "A wide-angle split step algorithm for the parabolic equation models," *JASA Suppl.* 1 83, 1983.

Tolstoy, A., *Matched Field Processing For Underwater Acoustics,* World Scientific, River Edge, NJ, 1993.

Urick, R.J., *Principles of Underwater Sound,* Kingsport Press, New York, NY, 1975.

INITIAL DISTRIBUTION LIST

No. copies

1. Defense Technical Information Center.....2
   8725 John J. Kingman Rd., STE 0944
   Ft. Belvoir, VA 22060-6218

2. Dudley Knox Library.....2
   Naval Postgraduate School
   411 Dyer Rd.
   Monterey, CA 93943-5101

3. Chairman, Code EC.....1
   Department of Electrical and Computer Engineering
   Naval Postgraduate School
   Monterey, CA 93943-5121

4. Dr. Kevin B. Smith, Code PH/Sk.....2
   Physics Department
   Naval Postgraduate School
   Monterey, CA 93943-5117

5. Dr. Ching-Sang Chiu, Code OC/Ci.....1
   Oceanography Department
   Naval Postgraduate School
   Monterey, CA 93943-5122

No. Copies

6. Dr. Ralph Hippenstiel, Code EC/Hi.....1
   Department of Electrical and Computer Engineering
   Naval Postgraduate School
   Monterey, CA 93943-5121

7. Stephen Greineder.....2
   Naval Undersea Warfare Center, Division Newport
   Code 2121, Bldg. 1320, Room 380
   Newport, RI 02841

8. Commander German Submarine Flottilla.....1
   Am Ort 6
   24340 Eckernfoerde
   Germany

9. LT. Joachim Brune.....2
   German Submarine Flottilla
   Am Ort 6
   24340 Eckernfoerde
   Germany